行政院國家科學委員會專題研究計畫　期中進度報告

彈性應變對自組式量子點光電特性之影響(2/3)

計畫類別：個別型計畫
計畫編號：NSC93-2212-E-002-015-
執行期間：93 年 08 月 01 日至 94 年 07 月 31 日
執行單位：國立臺灣大學應用力學研究所

計畫主持人：郭茂坤

計畫參與人員：林資榕、洪國彬、朱孝龍、林德焜

報告類型：精簡報告
報告附件：出席國際會議研究心得報告及發表論文
處理方式：本計畫可公開查詢

中　華　民　國 94 年 5 月 30 日

一、中文摘要：

半導體元件的光電特性決定於元件的能帶結構，而量子點中磊晶層之應變將造成半導體導電帶特徵能量的改變，進而影響電子躍遷難易度。本年度計畫以有限元素法套裝軟體分析砷化銦/砷化鎵自組式量子點(InAs/GaAs self-assembled quantum dot)，因晶格不匹配所引致的應變場，進而探討應變場對導電帶的特徵能量與電子機率密度函數分佈之影響。本研究以線彈性力學與初始應力理論利用FEMLAB，配合真實製程之模擬流程估算量子點內的應變分佈，再將應變效應加入薛丁格方程式，同樣以有限元素法予以分析。並澄清該系列文獻對應變的定義，同時發現考慮砷化銦鎵量子點中的銦之濃度後，模擬的應變場與實驗結果十分吻合；亦即對於應變場模擬而言，量子點中的銦之濃度為不可忽略的因素。

本計畫考慮材料之異向性並將應變場效應，藉由變形勢能，加入薛丁格方程式中，而同樣以有限元素法予以分析，藉此評估應變效應對於導電帶的特徵能量與電子機率密度函數分佈之影響，進而得到能帶間的躍遷能量(1.1 ~ 0.84 eV)與發光波長(1.13 ~ 1.48μm)。

關鍵詞：自組式量子點、應變場、有限元素法、薛丁格方程式

Abstract

In this year's project, the models based on linear elasticity and initial stress theory are successfully developed to evaluate the strain fields in the InAs/GaAs quantum dot nanostructures. The lattice mismatch in heterostructures induce the initial stress in quantum dots, and it will further lead to elastic deformation which calculated by finite element package—FEMLAB.

The Schrödinger equation, including the strain-induced potential is also solved by finite element method. The solutions consist of the eigenenergy and the probability density function of the conduction band.

The material properties of InGaAs quantum dots are assumed to depend on indium concentrations ($c(x,z)$). The strain distributions obtained by using the FEM have good agreement with experimentally data through HREM imaging.

Our results show that the energies of interband transitions and emission light's wavelength are 1.1 ~ 0.84 eV and 1.13 ~ 1.48μm, respectively.

Keywords：Self-assembled quantum dot, Strain field, FEM, Schrödinger equation.

二、研究目的：

由於半導體技術快速蓬勃地發展，使得光電與通訊元件之相關產業必需將產品微小化以增加競爭力，這也趨使半導體元件由早期的微米進入奈米尺寸的紀元，其中以半導體奈米結構－量子點，最受青睞 [1]。量子點是一種以厚度僅數奈米的幾種不同材料所做成，且三個維度均受侷限之微結構。受到侷限之影響，量子點內的能階量化，電子將被侷限在趨近於「點」的尺度內，因此量

子點可視為理想之零維度電子系統。同時，由於此種三維均受侷限之微結構所造成的量子能階類似於原子能階現象，因而又稱為人造原子 [2-3]。

量子點元件的發光功率，與量子點的密度有極大的關係；目前能較成功得到高密度量子點的方法，係利用變形磊晶技術以成長自組式量子點。而自組式量子點內變形磊晶層之應變，將直接影響半導體的導電帶與價電帶之結構及分佈，進而影響量子點內部的及其鄰近之電子的特性以及元件的光電性質。應變場與量子點及基材的晶格不匹配、材料的彈性係數、量子點的形狀、以及量子點的位置等因素有著密切的關係。

目前對於評估量子點與臨近母體間的彈性應變之理論及方法，仍眾說紛紜未有定論。常用的方法有三種，分別為：(1)考慮內含物的解析解 [4-6]、(2)有限元素法 [7-10]與(3)原子模型法 [11-13]。其中，內含物解析解，僅適用於簡單的量子點形狀(例如：球體)；而有限元素法雖無法提供通解，卻是有效率且適合各種量子點形狀的彈性變形場計算方法；原子模型法雖有不用建構在連體力學基礎上的優點，卻須有精確的原子間位能，且因量子點系統所需的原子數目甚多(約數萬個以上)，須耗費大量的計算量。前二種方法是由巨觀的連續體理論所發展；第三種方法則是從微觀的原子理論出發。以工程效率而言，有限元素法本身發展較為成熟且計算方便。

本計畫以線彈性力學與初始應力理論模擬異質材料晶格不匹配所引致應變現象；接著利用 Pikus-Bir Hamiltonian [14-15]，並配合有限元素法分析量子點的特徵能量與電子機率密度函數，探討應變場對導電帶及價電帶的特徵能量與電子機率密度函數分佈之影響。

三、研究方法：

3.1 應變場分佈

半導體異質結構係由兩種或以上的半導體材料磊晶而成。異質結構的形成可視為兩種單晶界面原子的結合，以本報告為例，交界面兩邊分別為基材 GaAs 與量子點材料 InAs 之元素化合物，如圖 1 所示。兩材料緊密砌合時，交界面處會因晶格的不匹配而產生應變，一般定義晶格不匹配常數為 [16]

$$\varepsilon_0 = \frac{a_s - a_d}{a_d} \quad , \qquad (1)$$

其中 a_d 、a_s 分別為量子點材料與基板材料的晶格常數。

本年度計畫採用初始應力理論來計算應變場，並改善模擬應變的流程。在真實的製程中，覆蓋層(cap layer) 乃於量子點生成後再蒸鍍上去，換言之，覆蓋層與量子點並無晶格不匹配的現象。晶格不匹所產生的初始應力，其表示式為

$$\sigma_0 = (C_{11} + C_{12} - 2C_{12}^2 / C_{11})\varepsilon_0 \qquad (2)$$

上式中的第一、二項乃二維晶格不匹配所產生，第三項則是薄松比效應造成，C_{11} 及 C_{12} 為彈性係數，此初始應力會進一步影響應變場的分佈。

在製程模擬上乃先考慮一含濕潤層(wetting layer)但未含覆蓋層之裸露型量子點模型如圖 1(a) 所示，並以有限元素軟體—FEMLAB 計算應變場; 接著再將覆蓋層加入形成埋藏型量子點，並將裸

露型量子點模型之應變場當成埋藏型量子點(圖 1(b))之初始應變，再利用有限元素軟體，求得整個量子點元件內的應變場。

3.2 電子結構

欲求得電子於導電帶之能量，其電子在量子點晶體中必須滿足薛丁格方程式(Schrödinger equation)：

$$\left[-\frac{\hbar^2}{2m^*}\left(\frac{\partial^2}{\partial x^2}+\frac{\partial^2}{\partial y^2}+\frac{\partial^2}{\partial z^2}\right)+V(x,y,z)\right]\psi(x,y,z) = E\psi(x,y,z) \quad (3)$$

方程式(3)中之$\hbar$為普蘭克常數除以2π，m^*為電子有效質量，$V(x,y,z)$為量子點結構的位能函數，E與$\psi(x,y,z)$分別為系統的特徵能量與其對應的電子機率密度函數。

本計畫考慮量子點的位能$V(\mathbf{r})$為

$$V(\mathbf{r}) = V_{\text{band}}(\mathbf{r}) + V_{\text{strain}}(\mathbf{r}) \quad , \quad (4)$$

其中，$V_{\text{band}}(\mathbf{r})$、$V_{\text{strain}}(\mathbf{r})$分別為導電帶的能帶差與應變引致的位能函數。而異質結構$In_cGa_{1-c}As/GaAs$的導電帶能帶差為

$$V_{band}(\mathbf{r}) = \begin{cases} 0 \ \text{V} & \mathbf{r} \in \text{InAs} \\ 0.84\,\text{eV} & \mathbf{r} \in \text{GaAs} \end{cases} . \quad (5)$$

根據 Pikus-Bir Hamiltonian [14-15] 理論，應變引致的位能函數可表示為

$$V_{\text{strain}} = a_c\left(\varepsilon_{xx}+\varepsilon_{yy}+\varepsilon_{zz}\right) \quad , \quad (6)$$

其中，a_c為變形位能(deformation potential) 。因此，將上節數值模擬所得之應變場代入方程式(6)，並結合方程式(4)、(5)即可求得量子點結構的位能函數，再利用有限元素法求解方程式(3)，如此便可估算出應變對導電帶特徵能量及電子機率密度函數分佈之影響。

四、結果與討論：

本年度計畫利用有限元素法套裝軟體—FEMLAB 分析 III-V 族半導體 InAs/GaAs 自組式量子點受晶格不匹配影響產生之應變分佈，進而探討應變對量子點的特徵能量與電子機率密度函數之影響。

由於 Kret 等人 [17-19] 研究發現，蒸鍍量子點材料於基材上時，基材溫度大於 420℃時所生成的量子點為三元化合物，故晶格常數、彈性係數、變形位能…等，依銦的濃度不同而有所差異。

為了驗證模擬的正確性，建構一與文獻上 [17] 相同的量子點薄片(如圖 2)，進行模擬應變場之分析，其結果與文獻吻合，如圖 3、4 所示。由此確立模擬方法的可行性與正確性。

圖 5、6 為利用異向性材料分析裸露型、埋藏型量子點時所得之結果，由圖中可知道，裸露型與埋藏型量子點的應變場分佈相當接近，較大的差異性產生於量子點頂端附近，這是因為覆蓋層的加入(埋藏型量子點)，致使量子點表面附近的應力、應變有重新分佈的情況。本計畫使用裸露型、埋藏型量子點模擬之結果，其ε_{xx}於量子點內仍為壓縮應變，於基板、覆蓋層則為拉伸應變，與文獻上的現象一致，但模擬結果顯示，較大的拉伸應變產生在基板，而不是覆蓋層，此結果與文獻上的結果相反。此外，裸露型、埋藏型量子點模擬所得之

ε_{zz}，與文獻上的結果相較之下，則有極大的差別，此乃因為使用裸露型、埋藏型量子點進行模擬時，覆蓋層對量子點應變場的影響十分有限，故ε_{zz}於量子點內幾乎全為拉伸應變；反觀文獻上的作法，覆蓋層對量子點的影響極為顯著，因而造成ε_{zz}於量子點頂端附近，有極大的壓縮應變。

圖 7 (a)及(b)分別為以異向性材料分析裸露型、埋藏型量子點元件受到應變場作用時，基態能階所對應之機率密度函數分佈圖。對於導電帶而言，其機率密度函數呈球形分佈於量子點內。圖 8(a)及(b)則分別為裸露型、埋藏型量子點元件第一激發態能階所對應之機率密度函數分佈圖。其機率密度函數呈球形雙侷限於量子點角落處。

五、結論：

本年度計畫重新解釋文獻上利用「高解析影像處理法」所求得的砷化銦鎵量子點應變場其定義為何，並說明該定義與真實應變場的定義有所出入。同時成功利用有限元素法，模擬砷化銦鎵量子點之應變場分佈，並將模擬結果與文獻上的結果，相互比較，得到極佳的吻合度。因此，對於應變場模擬而言，量子點中銦濃度的分佈，實為一不可忽略的因素。

針對砷化銦量子點應變場的模擬步驟，本年度提出更為貼近製程的分析方法，亦即區分為兩種模型進行模擬。(a)裸露型量子點：考慮未含覆蓋層之量子點，求其應變場分佈；(b)埋藏型量子點：先計算出未含覆蓋層量子點之應變場，再將此應變場視為起始應變場，代入含覆蓋層之量子點模型中，最終求得其應變場之分佈。

相較於依照文獻上模擬應變場的作法，進而所估算出的基態躍遷能量，本文改進後的應變場模擬方法，進而所估算的量子點基態躍遷能量，與實驗上的結果較為相近，且躍遷能量隨著量子點體積的增加而減小，此現象與文獻上利用PL 實驗所量測到的現象一致。本文估算的基態躍遷能量大小約為1.1 ~ 0.84 eV，亦即發光波長為1.13 ~ 1.48μm，此一波段位於紅外線光譜(infrared spectrum)上，因此，砷化銦/砷化鎵量子點可應用於紅外線偵測器的領域上。

六、文獻參考：

[1] D. Bimberg, M. Grundmann & N. N. Ledentsov, *Quantum Dot Heterostructures*, John Wiley & Sons, New York (1999).

[2] P. Harrison, *Quantum Wells, Wires and Dots: theoretical and computational physics*, John Wiley & Sons, New York (2000).

[3] T. Chakraborty, *Quantum Dots: a survey of the properties of artificial atoms*, Elsevier, Amsterdam (1999).

[4] V. A. Shchukin, D. Bimberg, V. G. Malyshkin & N. N. Ledentsov, Vertical correlations and anti- correlations in multisheet arrays of two dimensional islands, Phys. Rev. B **57**, 12262 (1998).

[5] D. Andreev, J. R. Downes, D. A. Faux

& E. P. O'Reilly, Strain distributions in quantum dots of arbitrary shape, J. Appl. Phys. **86,** 297 (1999).

[6] G. S. Pearson & D. A. Faux, Analytical solutions for strain in pyramidal quantum dots, J. Appl. Phys. **88**, 730 (2000).

[7] T. Benabbas, Y. Androussi & A. Lefebvre, A finite-element study of strain fields in vertically aligned InAs islands in GaAs, J. Appl. Phys. **86**, 1945 (1999).

[8] G. Muralidharan, Strains in InAs quantum dots embedded in GaAs: A finite element study, Jpn. J. Appl. Phys. **39**, L658 (2000).

[9] H. T. Johnson, L. B. Freund, C. D. Akyüz & A. Zaslavsky, Finite element analysis of strain effects on electronic and transport properties in quantum dots and wires, J. Appl. Phys. **84**, 3714 (1998).

[10] L.B. Freund & H.T. Johnson, The influence of strain on confined electronic states in semiconductor quantum structures, J. Mech. Phys. Solids **38**, 1045 (2001).

[11] M. Tadic, F. M. Peeters, K. L. Janssens, M. Korkusinski & P. Hawrylak, Strain and band edges in single and coupled cylindrical InAs/GaAs and InP/InGaP self-assembled quantum dots, J. Appl. Phys. **92**, 5819 (2002).

[12] C. Pryor, J. Kim, L. W. Wang, A. J. Williamson & A. Zunger, Comparison of two methods for describing the strain profiles in quantum dots, J. Appl. Phys. **83**, 2548 (1998).

[13] M. E. Bachlechner, A. Omeltchenko, A. Nakano, R. K. Kalia, P. Vashishta, I. Ebbsjö, A. Madhukar & P. Messina, Multimillion-atom molecular dynamics simulation of atomic level stresses in Si(111)/Si3N4(0001) nanopixels, Appl. Phys. Lett. **72**, 1969 (1998).

[14] G. E. Pikus and G. L. Bir, Effects of deformation on the hole energy spectrum of gernasium and silicon, Sov. Phys. Solid State **1**, 1502-1517 (1960).

[15] G. E. Pikus and G. L. Bir, *Symmetry and Strain-Induced Effects in Semiconductors*, Wiley New York (1974).

[16] L. B. Freund, The mechanics of electronic materials, J. Mech. Phys. Solids **37**, 185 (2000).

[17] S. Kret, T. Benabbas, C. Delamarre, Y. Androussi, A. Dubon, J.Y. Laval and A. Lefebvre, High resolution electron microscope analysis of lattice distortions and In segregation in highly strained $In_{0.35}Ga_{0.65}As$ coherent islands grown on GaAs(001), J. Appl. Phys. 86 1988 (1999).

[18] S. Kret, C. Delamarre, Atomic-scale mapping of local lattice distortions in highly strained coherent islands of $In_xGa_xAs/GaAs$ by high resolution electron microscopy and image processing, J.Y. Laval and A. Dubon, Philos. Mag.

Lett. 77, 249 (1998).

[19] S. Kret, P. Ruterana, A. Rosenauer and D. Gerthsen, Extracting quantitative information from high resolution electron microscopy, Phys. Stat. Sol. (b) 227, 247 (2001).

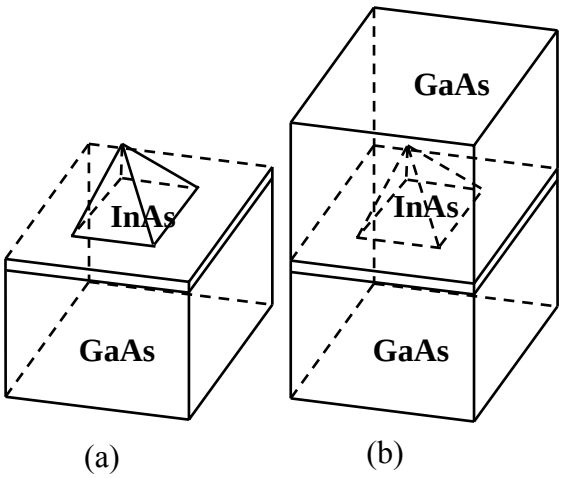

圖 1(a)裸露型量子點 (b)埋藏型量子點。

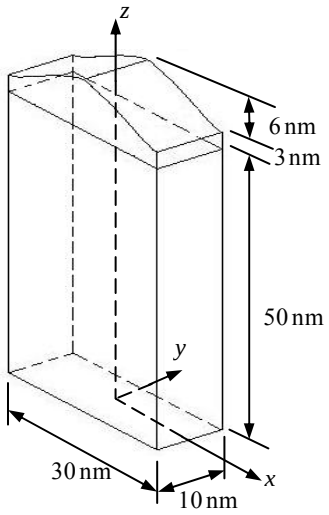

圖 2 砷化銦鎵量子點薄片幾何模型圖。

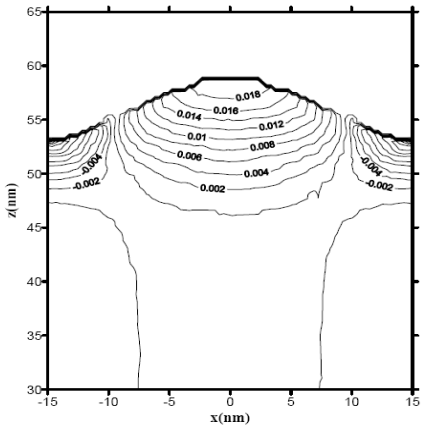

圖 3 初始應力理論模擬 ε_{xx} 分佈圖。

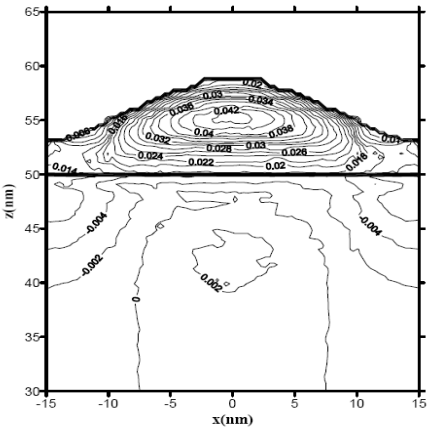

圖 4 初始應力理論模擬 ε_{zz} 分佈圖。

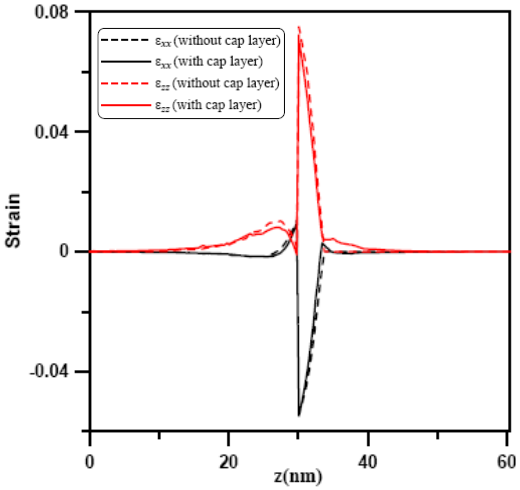

圖 5 量子點元件(h=3nm、b=12nm)，沿 z 軸之應變場分佈圖。

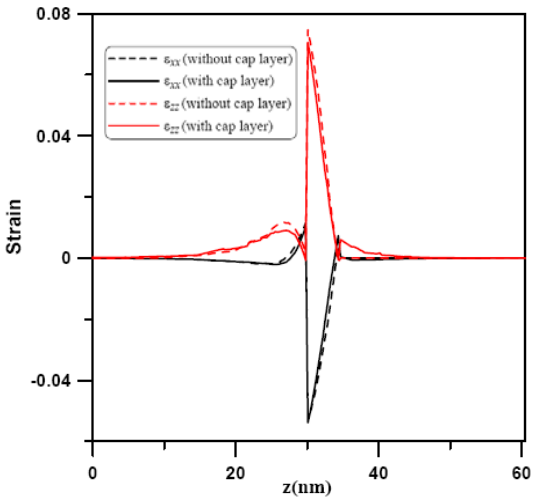

圖 6 量子點元件(h=4nm、b=12nm)，沿z軸之應變場分佈圖。

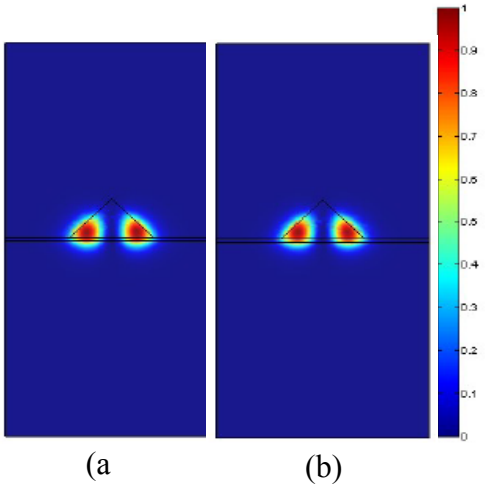

圖 8(a)裸露型量子點、(b)埋藏型量子點第一激發態能階之機率密度函數分佈函數分佈圖。

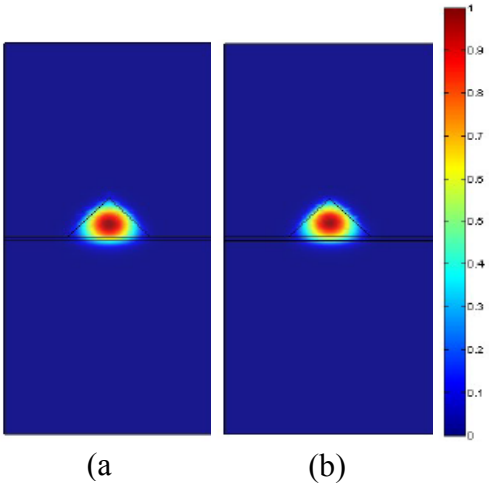

圖 7 (a)裸露型量子點、(b)埋藏型量子點基態能階之機率密度函數分佈圖。

附註：本年度計畫之成果已發表於國內外期刊集學術會議論文，共 3 篇：

1. M. K. Kuo, T. R. Lin, B. T. Liao and C. H. Yu, 2005, Strain effects on optical properties of pyramidal InAs/GaAs quantum dots, Physica E: Low-dimensional Systems and Nanostructures, v. 26, 199-202. (SCI, EI).
2. M. K. Kuo, T. R. Lin, B. T. Liao and C. H. Yu, 2004, Optical properties of InAs/GaAs quantum dots grown by epitaxy, Proceedings of IMECE04, 2004 ASME International Mechanical Engineering Conference and Exposition, Anaheim, California, USA, IMECE2004-59941.
3. T. R. Lin, M. K. Kuo, B. T. Liao and K.P. Hung, 2004, Mechanical and optical properties of InAs/GaAs self-assembled quantum dots, Bulletin of the College of Engineering, National Taiwan University, v. 91, 3-14.

Available online at www.sciencedirect.com
SCIENCE DIRECT®
Physica E 26 (2005) 199–202
PHYSICA E
www.elsevier.com/locate/physe

Strain effects on optical properties of pyramidal InAs/GaAs quantum dots

M.K. Kuo*, T.R. Lin, B.T. Liao, C.H. Yu[1]

Institute of Applied Mechanics, National Taiwan University, Taipei, 106 Taiwan, ROC

Available online 23 November 2004

Abstract

Strain distribution and optical properties in a self-assembled pyramidal InAs/GaAs quantum dot grown by epitaxy are investigated. A model, based on the theory of linear elasticity, is developed to analyze three-dimensional induced strain field. In the model, the capping material in the heterostructure is omitted during the strain analysis to take into account the sequence of the fabrication process. The mismatch of lattice constants is the driving source of the induced strain and is treated as initial strain in the analysis. Once the strain analysis is completed, the capping material is added back to the heterostructure for electronic band calculation. The strain-induced potential is incorporated into the three-dimensional steady-state Schrödinger equation with the aid of Pikus–Bir Hamiltonian with modified Luttinger–Kohn formalism for the electronic band structure calculation. The strain field, the energy levels and wave functions are found numerically by using of a finite element package FEMLAB. The energy levels as well as the wave functions of both conduction and valence bands of quantum dot are calculated. Finally, the transition energy of ground state is also computed. Numerical results reveal that not only the strain field but also all other optical properties from current model show significant difference from the counterparts of the conventional model.

PACS: 73.61.−r; 73.21.La; 73.40.Gk

Keywords: Quantum dots; InAs/GaAs; Lattice constants mismatch; Induced strain; Pikus–Bir Hamiltonian

1. Introduction

Quantum dots (QDs), owing to its own three-dimensional quantum confinement, are found to have delta-function distributions of density of states, discrete energy levels, "atom-like" electronic states, etc., and hence have attracted substantial attention recently [1]. Self-assembled QDs (SAQDs) formed by strained epitaxy have shown the promising result in having a large array of quantum dots. On the other hand, SAQD formation is commonly observed in large mismatch epitaxy of chemically similar materials [1,2].

*Corresponding author. Fax: 2-3366-5631.
E-mail address: mkkuo@ntu.edu.tw (M.K. Kuo).
[1]Now at Chung-San Institute of Science and Technology, Taoyuan 325, Taiwan, ROC.

1386-9477/$ - see front matter © 2004 Elsevier B.V. All rights reserved.
doi:10.1016/j.physe.2004.08.052

Strain fields inside quantum-dot hetrostructures strongly affect the electronic properties and hence the optoelectronic properties in the vicinity of dots [3]. To understand the strain effects on optical properties of quantum dots, determination of the induced strain field in the dots and the surrounding matrix is necessary. Finite element analysis has been used to investigate the strain field in the quantum dot [4–6].

A single square-based pyramidal self-assembled InAs quantum dot buried in GaAs matrix is considered in the article as depicted in Fig. 1. The InAs is grown a thin wetting layer on (0 0 1) GaAs substrate during heteroepitaxy, followed by coherent island formation. Finally, the quantum-dot island is subsequently covered by additional deposition of substrate materials.

2. Strain field

Epitaxially grown SAQD heterostructures often consist of several materials with different lattice constants. It gives rise to strain fields in a quantum-dot nanostructure, and affects the optical properties of the quantum dots [6]. In-plane lattice, mismatch parameter is usually defined as

$$(\varepsilon_0)_{xx} = (\varepsilon_0)_{yy} = \frac{a_s - a_d}{a_d}, \tag{1}$$

where a_s and a_d are the lattice constants of the substrate and the dot materials, respectively, i.e.,

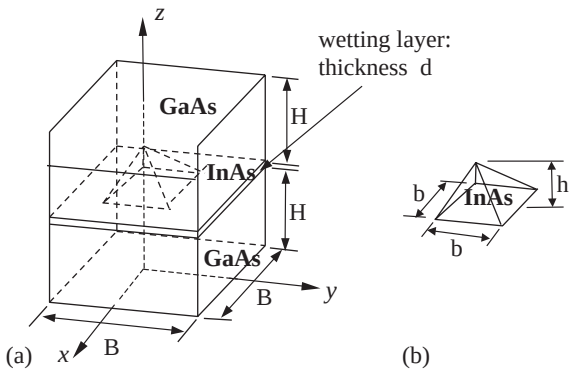

Fig. 1. Geometry of the quantum-dot system. (a) InAs/GaAs QD heterostructure, and (b) InAs quantum-dot island, where $B = H = 30$ nm, $d = 0.5$ nm, $b = 12$ nm, and $h = 6$ nm.

GaAs and InAs, and they will be taken as 0.565 and 0.605 nm, respectively, in the numerical computation of this article.

Notice that, the mismatch of lattice constants will induce further elastic deformation in the whole nanostructure system, namely, in both the substrate and the quantum-dot island. Thus the lattice mismatch parameter defined in Eq. (1) is not the only strain in the quantum-dot island. It will instead be treated as in-plane initial strain in the latter finite element analysis.

The out-of-plane initial strain, on the other hand, has never yet been as conclusive as its in-plane counterparts. It is a common belief that the in-plane initial strain in the epitaxy process will certainly accomplish with out-of-plane strain. In the article, the out-of-plane initial strain is taken as if it were strained elastically and in plane-stress state, which leads to

$$(\varepsilon_0)_{zz} = -\frac{2C_{12}}{C_{11}}(\varepsilon_0)_{xx}. \tag{2}$$

Here both GaAs and InAs are treated as cubic materials with three independent elastic moduli each, namely, C_{11}, C_{12}, and C_{44}.

In the article, parameters ε_0's are regarded as the initial normal strains in the x, y, and z directions in the latter finite element calculation. These initial strains in the wetting layer and the quantum-dot island will further induce the strain field in a SAQD system.

According to the theory of linear elasticity, the relationship among stresses σ_{ij}, total strains ε_{kl}, and initial strains can be expressed as

$$\sigma_{ij} = C_{ijkl}[\varepsilon_{kl} - (\varepsilon_0)_{kl}], \quad i,j,k,l = x,y,z, \tag{3}$$

where C_{ijkl} is the elastic moduli, and ε_0 is the normal initial strain described in Eqs. (1) and (2).

The wetting layer grows on the substrate during the quantum-dot fabrication process, and then further embedded in the capping material after quantum-dot island formation, as shown in Fig. 1. Since the capping material is deposited after the quantum-dot island has been formed, it should have never experience the deformation of quantum dot in the self-assembled process. Hence, the capping material is not included in the strain analysis.

In the stage of strain analysis, the quantum-dot heterostructure system is considered to consist of only quantum dot, wetting layer and substrate but not capping material. The mismatch of lattice constants of the heterostructure is the driving source for the induced strain. Once the strain analysis has been completed, the capping layer is then added into the system as if it is deposited after quantum-dot formation.

The adding of capping material is only for the purpose of solving the Schrödinger equation to obtain the electronic structure of the nanostructure system. This proposed model partially takes the sequence of fabrication process into account as compared to the conventional model where the capping material is considered as a body with other materials.

Figs. 2 and 3 show the normal strain ε_{xx} andε_{zz}, respectively, along the z-axis in quantum-dot nanostructures. It is not surprising that these strain components are discontinuous at the interface of the wetting layer and the substrate (i.e. InAs/GaAs interface).

Notice that, as seen from the figures, the strain filed ε_{xx} inside the dot is compressive while ε_{xx} is tensile. These reflect the fact that the lattice constant of InAs is larger than that of GaAs. From Figs. 2–3, it is easy to conclude that strain distributions obtained from the conventional and proposed models lead to significant difference.

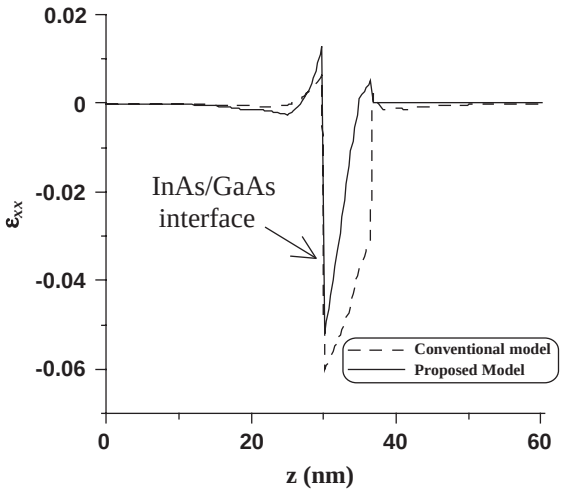

Fig. 2. Strain component ε_{xx} along the z-axis.

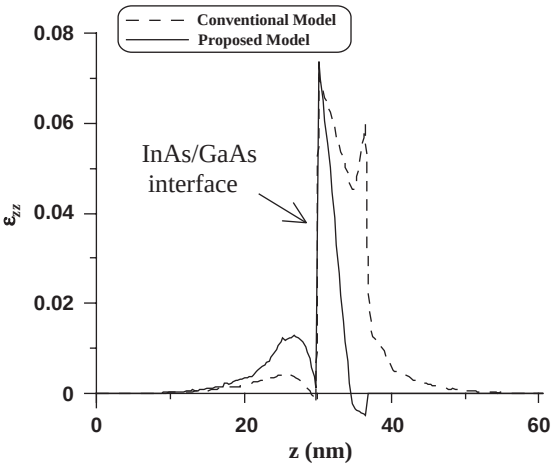

Fig. 3. Strain component ε_{zz} along the z-axis.

3. Optical properties

For strained quantum-dot nanostructures, the confinement potential can be written as a sum of energy offsets of the conduction band (or valence band), V_{band}, and the strain-induced potential, V_{strain}, as

$$V(\vec{r}) = V_{\text{band}}(\vec{r}) + V_{\text{strain}}(\vec{r}). \tag{4}$$

Since strain effects induce an extra potential field, it then alters the band structure and optical properties of the quantum-dot system. In spite of inhomogeneous distribution of induced strain (as depicted in Figs. 2–3), the Pikus–Bir Hamiltonian and the Luttinger–Kohn model [4] together with the computed strain field are employed as usual as an approximation to analyze strain-induced potentials in quantum dots.

The strain-induced potential along the z-axis is superimposed to energy band of bulk materials, as shown in Fig. 4. It is found that the strain effects on potentials of both the conduction and valence bands are non-negligible and non-uniform, especially, in the wetting layer and the quantum-dot regions.

Based on the computed energy and the computed wave function spectrum, the energy of interband optical transitions can readily be obtained. The calculated transition energies are in the

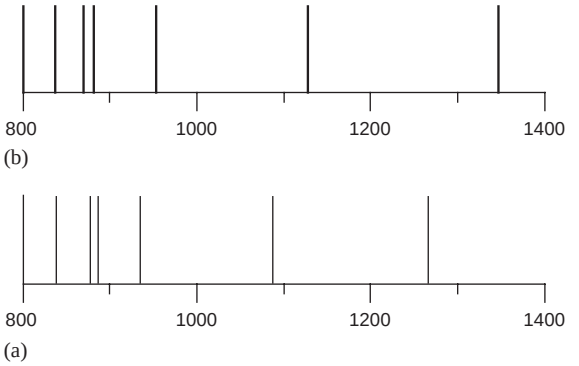

Fig. 4. The wavelengths of optical transition energies from 836 to 1353 nm via (a) the conventional model and (b) the proposed model.

range from 1.482 to 0.916 eV, which corresponds to 836–1353 nm in the optical wavelength spectrum as shown in Fig. 4. It shows that the wavelengths based on the strain fields from the proposed model differ significantly from their counterparts through the conventional model, especially for the cases of longer wavelength. It suggests that the proposed model of strain analysis might be necessary for the future optical analysis and applications.

4. Conclusions

In this article, a novel model based on the theory of linear elasticity with the aid of finite element analysis has been proposed to investigate the strain field as well as strain effects on optoelectronic properties of the pyramidal InAs/GaAs quantum-dot structures. In order to take into account the sequence of fabrication process the strain field in the heterostructure system without capping material was analyzed. The numerical results of the strain field from the proposed model have shown significant difference from the conventional model where the sequence of fabrication process was omitted.

The calculated strain field has also been used as an input for the electronic band structure calculation. The computed wavelengths of the optical transition energies ranged from 836 to 1353 nm. In the meantime, the wavelengths based on the strain fields from the proposed strain analysis have also differed significantly from the counterparts of the conventional strain analysis model. Hence the proposed strain analysis is necessary for the future optical analysis and applications.

Acknowledgement

This work is carried out in the course of research sponsored by the National Science Council of Taiwan under Grant NSC92-2212-E-002-072.

References

[1] D. Bimberg, M. Grundmann, N.N. Ledentsov, Quantum Dot Heterostructures, Wiley, New York, 1999.
[2] P. Harrison, Quantum Wells, Wires and Dots: Theoretical and Computational Physics, Wiley, New York, 2000.
[3] G.E. Pikus, G.L. Bir, Sov. Phys. Solid State 1 (1960) 1502.
[4] G. Muralidharan, Jpn. J. Appl. Phys. 39 (2000) L658.
[5] H.T. Johnson, L.B. Freund, C.D. Akyüz, A. Zaslavsky, J. Appl. Phys. 84 (1998) 3714.
[6] L.B. Freund, H.T. Johnson, J. Mech. Phys. Solids 38 (2001) 1045.

Proceedings of IMECE04
2004 ASME International Mechanical Engineering Congress and Exposition
November 13-20, 2004, Anaheim, California USA

IMECE2004-59941

OPTICAL PROPERTIES OF INAS/GAAS QUANTUM DOTS GROWN BY EPITAXY

M. K. Kuo, T. R Lin, B. T. Liao and C. H. Yu[1]
National Taiwan University, Institute of Applied Mechanics
No. 1 Sec. 4 Roosevelt Road, Taipei, 106, Taiwan, Rep. of China
Tel: +886-2-3366-5630, mkkuo@ntu.edu.tw

ABSTRACT

Strain effects on optical properties of self-assembled InAs/GaAs quantum dots grown by epitaxy are investigated. A new model based on the theory of linear elasticity is developed to analyze three-dimensional induced strain field. The model takes sequence of fabrication process of quantum-dot into account, where the mismatch of lattice constants between wetting layer and substrate is treated as initial strain first for the heterostructure system without capping material. The obtained total strain field is then treated as initial strain again for the whole heterostructure system with capping material. The computed strain from these two-steps analysis is then used as an input for the electronic band structure calculation. The numerical results show that strain field from this new model has significant difference from the usual model where the sequence of fabrication process is omitted.

The strain-induced potential is incorporated into the three-dimensional steady state effective mass Schrödinger equation with the aid of the Pikus-Bir Hamiltonian and Luttinger-Kohn formalism. Both the strain field and the solutions of the steady state Schrödinger equations are found numerically by using of a commercial finite element package. The energy levels as well as the wave functions of both conduction and valence bands of quantum dots are calculated. Finally, energy of interband optical transitions is obtained in numerical experiments.

Keywords: quantum dot, InAs/GaAs, induced strain, optoelectronic properties, Pikus-Bir Hamiltonian

INTRODUCTION

Quantum dots (QDs), which have delta-function distributions of density of states, discrete energy levels, and "atom-like" electronic states due to its three-dimensional quantum confinement, have recently attracted substantial attention [1, 2]. The optoelectronic efficiency of QD is strong related to the density of dots in the quantum dot array. Self-assembled QDs (SAQDs) formed by strained epitaxy have shown the promising result to have a large array of quantum dots. SAQD formation is commonly observed in large mismatch epitaxy of chemically similar materials. For example, the Stranski-Krastanow (SK) growth of InAs on GaAs first involves the growth of a "wetting layer" of 1~2 monolayer thick followed by coherent island formation [1-3]. The SAQDs may be buried by a further growth of the same materials as the underlying substrate.

The strain fields inside and in the neighborhood of SAQDs strongly affect the electronic properties in the vicinity of dots, and hence the optoelectronic properties [4-5]. For the optoelectronic properties in III-V semiconductor materials (such as InAs and GaAs), there are two predominated strain effects, namely changes of levels of the conduction band and valence band. The conduction band is only affected by the hydrostatic strain, often referred to as the dilatation or trace of the strain tensor. The valence levels can change both with hydrostatic and biaxial strains.

To understand the strain effects on optical properties of QD, determination of the induced strain field in the dots and the surrounding matrix is necessary. There have been three different main methods: (i) theory of inclusions based on the analytical solution of elasticity [6-8], (ii) finite element methods (FEM) [9-12], and (iii) atomistic modeling [13-14]. The theory of inclusions provides integral expressions for the elastic fields which can be integrated in closed forms for simplest inclusion shapes, e.g. cylindrical or spherical quantum dots. On the other hand, the interactions between the quantum dot and the surrounding material may not be fully encountered. FEM is a very versatile and effective numerical method. It can easily accommodate various theories and model quantum dots to different levels. Atomistic models might be more reasonable, at least theoretically, to model system in nano-scale provided that accurate interatomic potentials are available. Moreover, it requires a huge computing capacity to model quantum dots and the surrounding matrix.

In this article, a two-step novel model based on the theory of linear elasticity is developed to evaluate the strain field in the InAs/GaAs SAQD nanostructure. The model takes into account

[1] now at Chung-Shan Institute of Science and Technology, Taoyuan 325, Taiwan, ROC

the sequence of the fabrication process of the self-assembled quantum dots. The mismatch of lattice constants in the heterostructures induces the strain field which is then calculated with the aid of a commercial finite element package FEMLAB. The carrier confinement potential in the three-dimensional steady-state Schrödinger equation is modified by strain distribution. The equation is then solved again by FEMLAB. The solutions consist of energy levels and wave function spectra in SAQD nanostructures. The energy of interband optical transitions is also obtained in the numerical experiments. Finally, strain effects on optical properties in pyramidal InAs/GaAs quantum dot are discussed.

NOMENCLATURE

a_0	Lattice constant
a_c , a_v	Deformation potential constant of conduction band and valence band
a_d , a_s	Lattice constant of dot and substrate
b	Deformation potential constant of valence band
C_{ijkl}	Elastic stiffness tensor
E_n	Energy level
E_{BG}^{GaAs} , E_{BG}^{InAs}	Energy band gap for GaAs and InAs
ΔE_c	Band energy offset of conduction band
ΔE_v	Band energy offset of valence band
m^* , m_e	Carrier and Electron effective mass
$m_{hh,xy}$	Hole effective mass in the x (or y)-direction
$m_{hh,z}$	Hole effective mass in the z-direction
V	Confinement potential
V_{band}	Band energy offset
V_{band}^c	Band energy offset for conduction band
V_{band}^v	Band energy offset for valence band
V_{strain}	Strain-induced potential
V_{strain}^c	Strain-induced potential for conduction band
V_{strain}^v	Strain-induced potential for valence band
ε_{kl}	Strain tensor
$(\varepsilon_0)_{xx}$	Initial strain in the x-direction
$(\varepsilon_0)_{yy}$	Initial strain in the y- direction
$(\varepsilon_0)_{zz}$	Initial strain in the z-direction
$\gamma_1, \gamma_2, \gamma_3$	Luttinger-Kohn parameters
$\hbar$	Reduced Planck's constant
ψ_n	Wave function
σ_{ij}	Stress tensor

1 STATEMENTS OF THE PROBLEM

A single square-based pyramidal self-assembled InAs quantum dot buried in GaAs matrix is considered as depicted in the Fig. 1. The InAs is grown a thin wetting layer on (0 0 1) GaAs substrate during heteroepitaxy, followed by coherent island formation. Finally, the quantum dot island is subsequently covered by additional substrate materials.

Analysis of the strained SAQD nanostructure is divided into three parts in the article. First, a model based on the theory of linear elasticity is proposed to determine strain distribution in InAs/GaAs nanostructures via finite element calculation. Second, the strain effects on the carrier confinement potential in nanostructure are incorporated with the aid of Pikus-Bir Hamiltonian and Luttinger-Kohn formalism. Finally, the three-dimensional steady-state Schrödinger equation is solved numerically to obtain the energy levels and wave function spectra in SAQD.

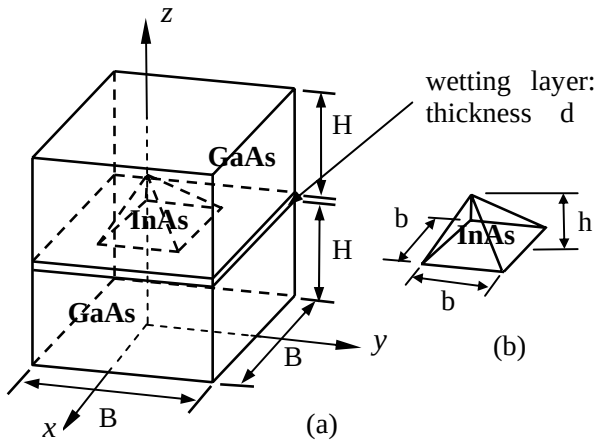

Fig. 1. Schematics and geometries of (a) the buried InAs/GaAs QD nanostructure and (b) the InAs quantum dot island; B = H = 30 nm, d = 0.5 nm, b and h are width and height of pyramid QD island, respectively. In the numerical examples in the article, b = 12 nm, and h = 6 or 3 nm.

2 STRAIN FIELD

Epitaxially grown semiconductor heterostructures, such as SAQDs, often consist of several materials with different lattice constants. The mismatch of lattice constants gives rise to strain fields in a quantum-dot nanostructure, which will affect the optical properties of the quantum dots [15]. In-plane lattice mismatch parameter is usually defined as

$$(\varepsilon_0)_{xx} = (\varepsilon_0)_{yy} = \frac{a_s - a_d}{a_d} \tag{1}$$

where a_s and a_d are the lattice constants of the substrate and the dot materials, respectively, i.e. GaAs and InAs, which will be taken as 0.565 nm and 0.605 nm, respectively, in the numerical computation of this article. Obviously, the lattice constant of the dot material (InAs) exceeds that of the substrate material (GaAs).

Notice that the mismatch of lattice constants will induce further elastic deformation in the whole nanostructure system, namely, in both the substrate and the quantum dot island. In other words, the lattice mismatch parameter defined in eq. (1) will not be the only strain in the quantum dot island. It will instead be treated as in-plane initial strain in the latter finite element analysis.

On the other hand, the out-of-plane initial strain has never yet been as conclusive as its in-plane counterparts. Though it is a common believe that the in-plane initial strain in the epitaxy process will certainly accomplish with out-of-plane

strain. In the article, the out-of-plane initial strain is taken as if it were strained elastically and in plane-stress state, which leads to

$$(\varepsilon_0)_{zz} = -\frac{2C_{12}}{C_{11}}(\varepsilon_0)_{xx} \quad (2)$$

Here both GaAs and InAs are treated as cubic materials with 3 independent elastic moduli each, namely, C_{11}, C_{12}, and C_{44}. Hence the 6×6 matrices of elastic moudi of both GaAs and InAs are in the form of

$$[C_{ij}] = \begin{pmatrix} C_{11} & C_{12} & C_{12} & 0 & 0 & 0 \\ C_{12} & C_{11} & C_{12} & 0 & 0 & 0 \\ C_{12} & C_{12} & C_{11} & 0 & 0 & 0 \\ 0 & 0 & 0 & C_{44} & 0 & 0 \\ 0 & 0 & 0 & 0 & C_{44} & 0 \\ 0 & 0 & 0 & 0 & 0 & C_{44} \end{pmatrix} \quad (3)$$

The numerical values of elastic moduli used in the article are complied as in Table 1.

In the article, the parameters $(\varepsilon_0)_{xx}$, $(\varepsilon_0)_{yy}$ and $(\varepsilon_0)_{zz}$ are regarded as the initial normal strains in the *x*, *y*, and *z*-directions, respectively, in the latter finite element calculation. These initial strains in the wetting layer and the quantum dot island will induce further the strain field in a SAQD system.

Table 1. Material properties [16]

Mechanical property	C_{11} (GPa)	C_{12} (GPa)	C_{44} (GPa)
GaAs	118.79	53.76	59.4
InAs	83.29	45.26	39.6
Deformation potential	a_c (eV)	a_v (eV)	b (eV)
GaAs	-7.17	1.16	-1.7
InAs	-5.08	1	-1.8
Effective mass[a]	$m_e(m_0)$	$m_{hh,xy}(m_0)$	$m_{hh,z}(m_0)$
GaAs	0.067	0.115	0.333
InAs	0.023	0.035	0.263

[a]From Luttinger-Kohn parameters $\gamma_1, \gamma_2, \gamma_3$

According to the theory of linear elasticity, the relationship among stresses σ_{ij}, total strains ε_{kl}, and initial strains can be expressed as:

$$\sigma_{ij} = C_{ijkl}\left[\varepsilon_{kl} - (\varepsilon_0)_{kl}\right] \quad i,j,k,l = x,y,z \quad (4)$$

where C_{ijkl} is the elastic moduli, and $(\varepsilon_0)_{kl}$ is the initial strain tensors described in eq. (1) and (2).

The linear elastic boundary value problem, arising from the mismatch in lattice constants between the wetting layer, the quantum-dot island and the substrate materials, is analyzed using a commercial finite element package FEMLAB. Appropriate boundary conditions are necessary in the analysis: all the nodes of the *x*- and *y*-outer surfaces are fixed against displacement in the normal direction due to periodic symmetric argument. The bottom outer surface is fixed against displacement in *z*-direction to avoid rigid body shift; whiles the upper surface is kept traction free. The displacement compatibility across the interface of island/substrate is satisfied automatically in the finite element formulation with displacement field as unknowns.

The wetting layer during the quantum-dot fabrication process grows on the substrate and then embedded in the capping material after quantum-dot island formation, as shown in Fig. 1. Here, the strain fields induced by mismatch of lattice constants in the heterogeneous quantum dot structure are investigated by using three different models.

Model I: The capping material with quantum dot and substrate are assumed to be acted as a body and deformed together. This is the conventional model used in almost all of the previous research works [9-11]. Notice that in the real fabrication process, the capping material is deposited after the quantum-dot island has been formed. Hence the capping material should have never been experienced the deformation of quantum-dot island in the formation process, i.e. the self-assembled process.

Model II: Since the capping material does not experience the deformation in the self-assembled process, the capping material is not considered in the strain analysis. In the stage of strain analysis, the quantum-dot heterostructure system is considered to consist of only quantum dot, wetting layer and substrate but not capping material. As in the model I, the mismatch of lattice constants of the heterostructure is the driving source for the induced strain. Once the strain analysis has been completed, the capping layer is then added into the system. The adding of capping material is only for the purpose of solving the Schrödinger equation to obtain the electronic structure of the nanostructure system. In this model, the capping material is consequently assumed to be unstrained. It is equivalently to neglect the re-distribution of strain in the quantum-dot system during the depositing process of the capping material. This model partially takes the sequence of fabrication process into account.

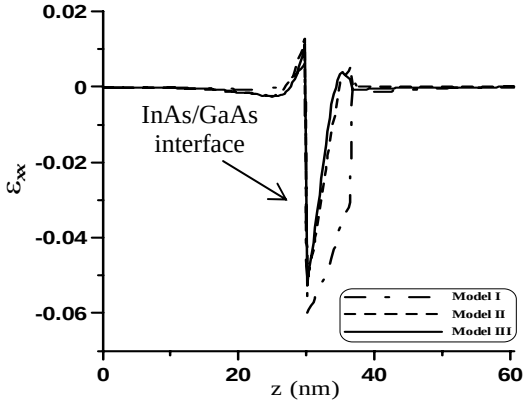

Fig. 2. Strain component ε_{xx} along the *z* -axis for the case of h = 6 nm.

Model III: A two-step strain analysis is used in this novel model. The strain analysis of the nanostructure system, without capping material, is performed in the first step as in the Mode II. The resulted total strain field is then taking again as initial strains to the whole quantum-dot nanostructure system, with capping material now, to analyze the further induced strain due to the capping process. The boundary conditions of pyramidal surface of the quantum dot are now changed from the original traction free condition to the continuity conditions of the

appropriate displacement and stress components. Hence the stress and strain will re-distribute in the nanostructure system. Again, the substrate, the wetting layer, and the quantum dot are analyzed together with the capping material. It is believed that this Model is much closer to the reality of the self-assembled fabrication process than the other two models.

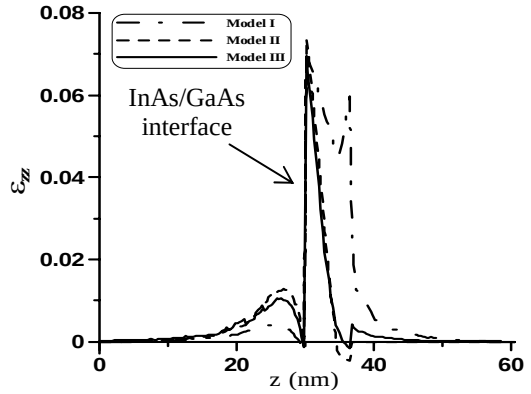

Fig. 3. Strain component ε_{zz} along the z -axis for the case of h = 6 nm.

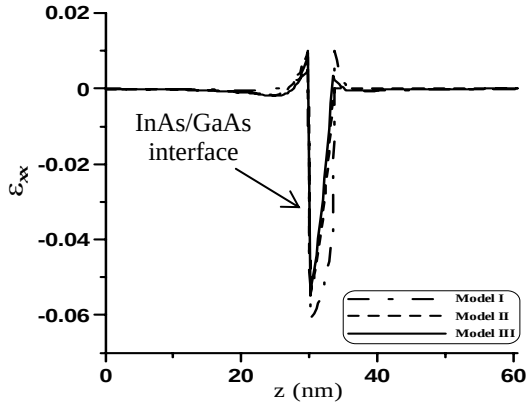

Fig. 4. Strain component ε_{xx} along the z -axis for the case of h = 3 nm.

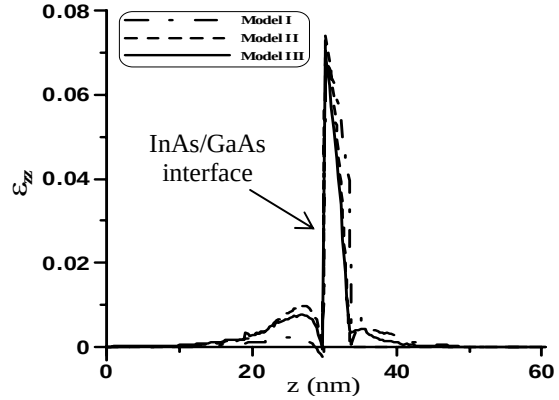

Fig. 5. Strain component ε_{zz} along the z -axis for the case of h = 3 nm.

In the article, there are two cases considered in the strain analysis, namely the cases that the height of pyramid quantum-dot island h = 6 and 3 nm, respectively. Figures 2 and 3 show the normal strain components ε_{xx} and ε_{zz}, respectively, along the z-axis in QD nanostructures for the case of h = 6 nm. While Fig. 4 and 5 are for the case of h = 3 nm. It is not surprised that these strain components are discontinuous at the interface of the wetting layer and the substrate (i.e. InAs/GaAs interface).

Notice that, as seen from the figures, the strain filed ε_{xx} inside the dot is compressive while ε_{zz} is tensile. These reflect the fact that the lattice constant of InAs is larger than that of GaAs. From Fig. 2-5, it is easily to conclude that strain distributions obtained from Model II and from Model III are almost identical, especially inside the quantum-dot island. It implies that the strain field inside the quantum-dot island is only slightly redistributed after the capping material has been deposited. It might also suggest that, to the first-order approximation of the strain field, the capping material can be neglected for simplicity. On the other hand, strains obtained from Model I and Model III leads to significant difference. Moreover, the bigger the quantum-dot is, the bigger the difference.

3 CONFINEMENT POTENTIAL

For strained quantum-dot nanostructures, the confinement potential can be written as a sum of energy offsets of the conduction band (or valence band), V_{band}, and the strain-induced potential, V_{strain}, as

$$V(\vec{r}) = V_{\text{band}}(\vec{r}) + V_{\text{strain}}(\vec{r}) \tag{5}$$

The band structure contribution is determined by considering the difference in band gap energies of the heterostructure constituent materials. Since strain effects induce an extra potential field, V_{strain}, it may then alter the band structure and optical properties of the quantum-dot system. In spite of inhomogeneous distribution of induced strain (as depicted in Fig. 2-5), the Pikus-Bir Hamiltonian together with the computed strain field and the Luttinger-Kohn model [4-5] are employed as usual as an approximation to analyze strain-induced potentials in quantum-dot nanostructures.

Since the conduction band level is only affected by the hydrostatic strain, strain-induced potential for the conduction band is expressed as [4]

$$V_{\text{strain}}^{\text{c}} = a_{\text{c}}\left(\boldsymbol{\varepsilon}_{xx} + \boldsymbol{\varepsilon}_{yy} + \boldsymbol{\varepsilon}_{zz}\right) \tag{6}$$

On the other hand, the valence level can change both with hydrostatic and biaxial strain; thus strain-induced potential for the valence band can be written as [5]

$$V_{\text{strain}}^{\text{v}} = a_{\text{v}}\left(\varepsilon_{xx} + \varepsilon_{yy} + \varepsilon_{zz}\right) - \frac{b}{2}\left(\varepsilon_{xx} + \varepsilon_{yy} - 2\varepsilon_{zz}\right) \tag{7}$$

where a_{c} is the deformation potential constant of conduction band; a_{v} and b denote the deformation potential constants of valence band. A list of material properties used, including the deformation potential constants, is compiled in Table 1.

By using of equations (6) and (7) together with the strain field computed from finite element calculation as above-mentioned in the previous section, the strain-induced potential along the z-axis is then superimposed to energy band of bulk materials, as shown in Fig. 6 for the case of h = 6 nm. It is found that the strain effects on potentials of both the conduction and valence bands are non-negligible and non-uniform, especially, in the wetting layer and the quantum-dot regions.

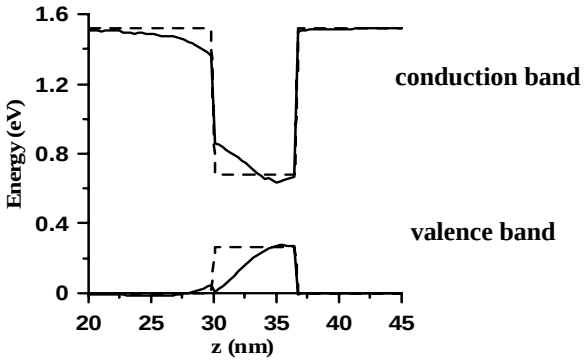

Fig. 6. Energy bands of the strained and unstrained InAs/GaAs heterostructures along the *z*-axis. Dash line and solid line are strained and unstrained potential profiles, respectively.

4 ELECTRONIC STRUCTURE

The behavior of individual carrier in QD nanostructures is governed by the three-dimensional steady state effective mass Schrödinger equation as :

$$\left[-\frac{\hbar^2}{2}\nabla_{\vec{r}}\left(\frac{1}{m^*}\right)\nabla_{\vec{r}}+V(\vec{r})\right]\psi_n(\vec{r})=E_n\,\psi_n(\vec{r}) \qquad (8)$$

where $\nabla_{\vec{r}}$ stands for the spatial gradient, $V(\vec{r})$ is the confinement potential field, m^* denotes the carrier effective mass, $\hbar$ is the reduced Planck's constant, and E_n and $\psi_n(\mathbf{r})$ are the n-th energy level and the corresponding wave function, respectively. The effective masses used are listed again in Table 1.

Equation (8) is also solved numerically by means of the same commercial finite element method package FEMLAB, in order to obtain energy levels and the wave functions in a QD nanostructure. The boundary conditions for the Schrödinger equation on the quantum dot/substrate interfaces are

$$\begin{cases}\psi_d=\psi_s\\ \dfrac{1}{m^*_{d_{n_i}}}\dfrac{\mathrm{d}\psi_d}{\mathrm{d}n}=\dfrac{1}{m^*_{s_{n_i}}}\dfrac{\mathrm{d}\psi_s}{\mathrm{d}n}\end{cases} \qquad (9)$$

where subscripts *d* and *s* correspond to the quantum dot and substrate regions, respectively, *n* denotes the normal directions of interfaces, a carrier effective mass is taken along the normal directions of interfaces. In addition, at the top of the capping layer, bottom of the substrate, and their outer surfaces, the wave functions are set to be zero.

Table 2. Energy levels (eV).

	E_{e0}	E_{e1}, E_{e2} [a]	E_{e3}	E_{h0}	E_{h1}, E_{h2} [a]	E_{h2}
I	0.559	0.778	0.844	0.001	0.127	0.135
II	0.469	0.725	0.833	0.031	0.156	0.173
III	0.457	0.720	0.831	0.039	0.158	0.174

[a] E_{e1}, E_{e2} and E_{h1}, E_{h2} are degeneracy of energy levels, respectively.

The calculated energy levels for the ground, the first excited, and the second excited states are summarized in Table 2. While the corresponding transition energies between each state are shown in Table 3. The transition energies are defined as sum of electron energy, hole energy, and band-gap energy. These transition energies are related to the peak of experimental photoluminescence (PL) spectrum. From Table 2, it is easily to notice that the confined energies computed from Model II and Model III give rise to nearly the same results. This phenomenon may reflect the fact of having similar strain distribution.

Table 3. Optical transition energies (eV).

	E_{e0-h0}	E_{e1-h1}, E_{e2-h2}	E_{e3-h3}
I	0.980	1.325	1.399
II	0.921	1.301	1.426
III	0.916	1.298	1.424

Based on the computed energy and the computed wave function spectrum, the energy of interband optical transitions can readily be obtained. The optical conductivity features peaks at particular wavelengths of light that are more strongly absorbed; these wavelengths in turn can be expected to be the strongest emission wavelengths. The calculated transition energies, for the case of h = 6 nm, are in the range from 1.482 eV to 0.916 eV which correspond to the wavelength of 836 nm ~ 1353 nm in the optical wavelength spectrum as shown in Fig. 7. It shows that the wavelengths based on the strain fields from Model III differ significantly from the counterparts via Model I, especially for the cases of longer wavelength. It suggests that the proposed two-step strain analysis, namely Model III, might be necessary for the future optical analysis and applications.

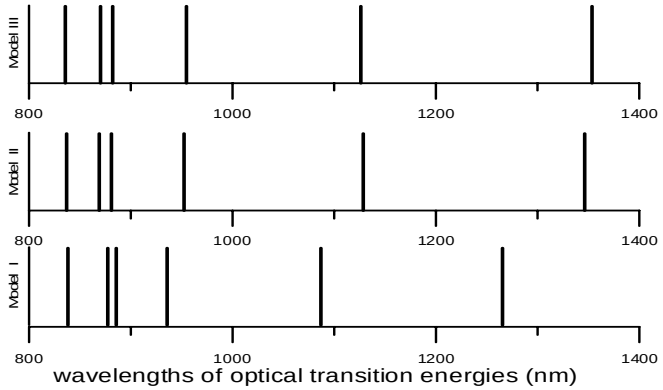

Fig. 7. The calculated wavelengths of optical transition energies from 836 nm to 1353 nm via three different model of strain analysis for the case of h = 6 nm.

Probability density function profiles, given by square of wave functions, namely $|\psi|^2$, for energy levels of the ground state in a quantum-dot nanostructure simulated by Model III, are shown in Fig. 8. Subfigures 8 (a) and (b) are the probability density function profiles corresponding to the electron energy level and the hole energy level, respectively. The probability density function distributions are confined almost entirely to the quantum-dot island region. And the distributions of the probability density function of electron energy levels are seem to be spherically symmetric within the whole island. On the other hand, the distributions of the probability density function of hole energy levels are likely to be more confined in the bottom of the island.

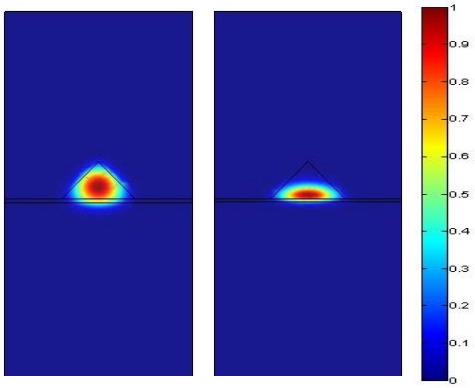

(a) (b)

Fig. 8. Probability density function profiles for energy levels of the ground state corresponding to (a) electron energy; (b) hole energy. The cross section is the *yz*-plane through the dot center.

6 CONCLUSION

In the article, a novel model based on the theory of linear elasticity with the aid of finite element analysis has been proposed to investigate the strain field as well as strain effects on optoelectronic properties of the self-assembled pyramidal InAs/GaAs quantum-dot structures. A two-steps strain analysis has been employed in the model to take into account the sequence of fabrication process of quantum dot. In the first step, the strain field in the heterostructure system without capping material was first analyzed, where the mismatch of lattice constants between the wetting layer and the substrate was the driving source and was treated as initial strain in the analysis. The obtained strain field has then been treated again as initial strain except for the complete heterostructure system with capping material now. The changes of the boundary conditions of pyramidal surface of the quantum-dot from traction free to the continuity conditions of the appropriate displacement and stress components served as other driving sources of strain in this step. The numerical results of the final strain field from this new novel model have shown significant difference from a conventional model where the sequence of fabrication process was omitted.

The calculated strain field from the two-steps analysis has also been used as an input for the electronic band structure calculation. Though the strain distribution in the quantum-dot nanostructures is not uniform, the Pikus-Bir Hamiltonian and the Luttinger-Kohn model have, nevertheless, been employed as usual as an approximation to analyze strain-induced potentials in quantum-dot nanostructures. The energy levels and the wave function distribution have been obtained by solving the three-dimensional steady state effective mass Schrödinger equation, including the strain-induced potential.

The computed wavelengths of the optical transition energies ranged from 836 nm to 1353 nm. In the meantime, the wavelengths based on the strain fields from the two-step analysis have also differed significantly from the counterparts via the conventional strain analysis model. Hence the proposed two-step strain analysis is necessary for future optical analysis and applications.

ACKNOWLEDGMENTS

This work is carried out in the course of research sponsored by the National Science Council of Taiwan under Grants NSC92-2212-E-002-072 and NSC93-2212-E-002-015.

REFERENCES

[1] Bimberg, D., Grundmann, M. and Ledentsov, N. N., 1999, *Quantum Dot Heterostructures*, John Wiley and Sons, New York.

[2] Harrison, P., 2000, *Quantum Wells, Wires and Dots: theoretical and computational physics***,** John Wiley and Sons, New York.

[3] Chakraborty, T., 1999, *Quantum Dots: a survey of the properties of artificial atoms*, Elsevier, Amsterdam.

[4] Pikus, G. E., and Bir, G. L., 1960, Effects of deformation on the hole energy spectrum of gernasium and silicon, Sov. Phys. Solid State, **1**, pp. 1502-1517.

[5] Pikus, G. E., and Bir, G. L., 1974, *Symmetry and Strain-Induced Effects in Semiconductors*, Wiley, New York.

[6] Shchukin, V. A., Bimberg, D., Malyshkin, V. G. and Ledentsov, N. N., 1998, Vertical correlations and anticorrelations in multisheet arrays of two dimensional islands, Phys. Rev. B, **57**, pp. 12262.

[7] Andreev, D., Downes, J. R., Faux, D. A., and O'Reilly, E. P., 1999, Strain distributions in quantum dots of arbitrary shape, J. Appl. Phys., **86,** pp. 297.

[8] Pearson, G. S., and Faux, D. A., 2000, Analytical solutions for strain in pyramidal quantum dots, J. Appl. Phys., **88**, pp.730.

[9] Benabbas, T., Androussi, Y. and Lefebvre, A., 1999, A finite element study of strain fields in vertically aligned InAs islands in GaAs, J. Appl. Phys., **86**, pp. 1945.

[10] Muralidharan, G., 2000, Strains in InAs quantum dots embedded in GaAs: A finite element study, Jpn. J. Appl. Phys., **39**, L 658.

[11] Johnson, H. T., Freund, L. B., Akyüz, C. D. and Zaslavsky, A., 1998, Finite element analysis of strain effects on electronic and transport properties in quantum dots and wires, J. Appl. Phys., **84**, pp. 3714.

[12] Freund, L. B., and Johnson, H. T., 2001, The influence of strain on confined electronic states in semi- conductor quantum structures, J. Mech. Phys. Solids, **38**, pp. 1045.

[13] Tadic, M., Peeters, F. M., Janssens, K. L., Korkusinski, M. and Hawrylak, P., 2002, Strain and band edges in single and coupled cylindrical InAs/GaAs and InP/InGaP self-assembled quantum dots, J. Appl. Phys., **92**, pp. 5819.

[14] Pryor, C., Kim, J., Wang, L. W., Williamson, A. J., and Zunger, A., 1998, Comparison of two methods for describing the strain profiles in quantum dots, J. Appl. Phys., **83**, pp.2548.

[15] Freund, L. B., 2000, The mechanics of electronic materials, J. Mech. Phys. Solids, **37**, pp. 185.

[16] Chuang, S. L., 1995, *Physics of optoelectronic devices*, John Wiley and Sons, New York.

國立臺灣大學「台大工程」學刊　第九十一期　民國九十三年六月　第 3–14 頁
Bulletin of the College of Engineering, N.T.U., No. 91, June 2004, pp. 3–14

MECHANICAL AND OPTICAL PROPERTIES OF InAs/GaAs SELF-ASSEMBLED QUANTUM DOTS

砷化銦／砷化鎵自聚式量子點之機械與光學特性

林 資 榕[*]　郭 茂 坤[**]　廖 柏 亭[†]　洪 國 彬[*]

Tzy-Rong Lin　*Mao-Kuen Kuo*　*Bo-Ting Liao*　*Kuo-Pin Hung*

[*]博士生　[**]教授　[†]碩士班研究生
國立台灣大學應用力學研究所

[*] Ph.D. candidate　[**] Professor　[†] Graduate student
Institute of Applied Mechanics, National Taiwan University, Taipei, Taiwan 10617, R.O.C.

摘　要

本文旨在介紹自聚式量子點的特性、製程與應用，並以砷化銦／砷化鎵 (InAs/GaAs) 為基礎的自聚式量子點為例，分析其機械及光學特性。文中首先以線彈性力學理論，配合有限元素法套裝軟體，估算量子點內因異質材料間的晶格不匹配所引致的應變場分佈；再將此應變場效應，經由變形勢能，加入於薛丁格方程式中，而同樣以有限元素法分析，藉以評估應變效應對於導電帶、價電帶的特徵能量與電子、電洞機率密度函數分佈之影響，進而得到能帶間的電子躍遷能量與發光波長。由模擬結果得知，電子躍遷能量隨著量子點尺寸的增大而減小，亦即發光波長隨著量子點的增大而變長，此結果與文獻上的現象十分吻合。

關鍵詞： 自聚式量子點、應變場、有限元素法、薛丁格方程式。

Abstract

This article reviews the properties, growth mechanics, and applications of self-assembled quantum dots. A model based on theory of linear elasticity is developed to analyze the strain field induced by lattice-mismatch between quantum dot and substrate. The induced strain field is then incorporated, with the aid of the Pikus-Bir Hamiltonian and Luttinger-Kohn formalism, into the three-dimensional steady-state effective mass Schrödinger equation. Both the strain field and the solutions of the Schrödinger equations are solved numerically by using of a commercial finite element package. The energy levels as well as the wave functions of both conduction and valence bands of quantum dots are calculated. Finally energies of interband optical transitions are then obtained in numerical experiments. Numerical results show that the transition energy decreases with increasing of the dot size. This phenomenon agrees well with the previous results reported by others.

Keywords: self-assembled quantum dot, strain field, finite element method (FEM), schrödinger equation.

1. INTRODUCTION

One of the significant features of semiconductors is the energy gap which separates the conduction and valence energy bands. For instance, the color of light emitted by semiconductor materials is determined by the width of the energy gap. In semiconductors of macroscopic sizes, *i.e.*, bulk semiconductors, the widths of energy gaps are fixed parameters controlled by the semiconductors' identities.

On the other hand, in the cases of nanometer-sized semiconductors, with sizes around 10-100 nanometers, the situations change. It has been demonstrated that this range of the geometrical sizes of semiconductors is comparable with the spatial extents of the electronic wave functions. As results of the geometrical constraints, electrons will "sense" the presence of the geometrical boundaries of semiconductors and will respond to change accordingly by adjusting their energy. This phenomenon is known as the quantum confined

effect.

If one should define quantum dot exactly, it certainly has to be set out from the point of view of quantum mechanics. Since electrons have wave-particle duality, the property of electron waves depends on its Fermi-wavelength. In general, the wavelength of the electron is smaller than the size of the bulk material but comparable or even larger than the one of nano-scaled material. Therefore, the quantum confined effect is obvious. Usually, the nano-scaled materials have better acoustic, optic, electric, and thermal properties.

A quantum well is, in fact, a potential well which is very small in size. The "well" is like a box in which electrons would be trapped, in much the same way that light is trapped between mirrors. By making layers of different semiconductor materials, it is then possible to make a particular layer acts as a trap for electrons. It can take one more step further, by making a thin "wire", but not a layer, of the preferred semiconductor. These trapped electrons are then in two-dimensional quantum confinement (called quantum wire).

Quantum dots (QDs) are solid-state structures made of heterogeneous semiconductors or metals being capable of confining a countable, small numbers of electrons into a small space. The confinement of electrons is achieved by setting some insulating materials around a central, well conducting region. The densities of states for cases of bulk semiconductors, quantum wells, quantum wires and quantum dots are quite different as shown schematically in Fig. 1. Quantum dots have also been called artificial atoms.

Rapid developments on semiconductor technologies, especially various epitaxy techniques for preparing molecular layers of materials and lithography techniques for fabricating densely packed electrical circuits, have resulted in new possibilities for a creation of artificially ultra-small physical systems, say of sizes of couple nm, with controlled properties. In this unique situation, the manipulation of materials, however, meets with limitations imposed on small systems by quantum mechanics. Description of extremely small systems taken from macroscopic physics is irrelevant, as regards both optoelectronic properties and mechanical behavior. In this article, the size of QD is around 10's nm, hence the macroscopic viewpoint might still be feasible.

One of the most important factors driving the current active researches in quantum effect is the rapidly expanding on semiconductor band-gap engineering capability [1] offered by modern epitaxy, such as molecular beam epitaxy (MBE) and metallorganic chemical vapor deposition (MOCVD). MBE is a vacuum deposition technique carried out in an ultrahigh vacuum environment. It is a versatile technique for growing thin epitaxial structures made of metals, semiconductors and insulators.

MBE growth is carried out under conditions far from thermodynamic equilibrium, and it is governed mainly by the kinetics of the surface processes occurring when the impinging beams interact with the outermost atomic layers of the substrate crystal. MBE has a unique advantage over all other epitaxial growth techniques in significantly precise control on the beam fluxes and growth conditions.

In the cases of heteroepitaxial growth, one of the most important growth modes is so-called Stranski-Krastanow (SK) growth mode. The formation of Stranski-Krastanow islands is closely related to an epitaxial misfit and the accumulation of elastic strain energy in the epilayer. Strain relaxation takes place

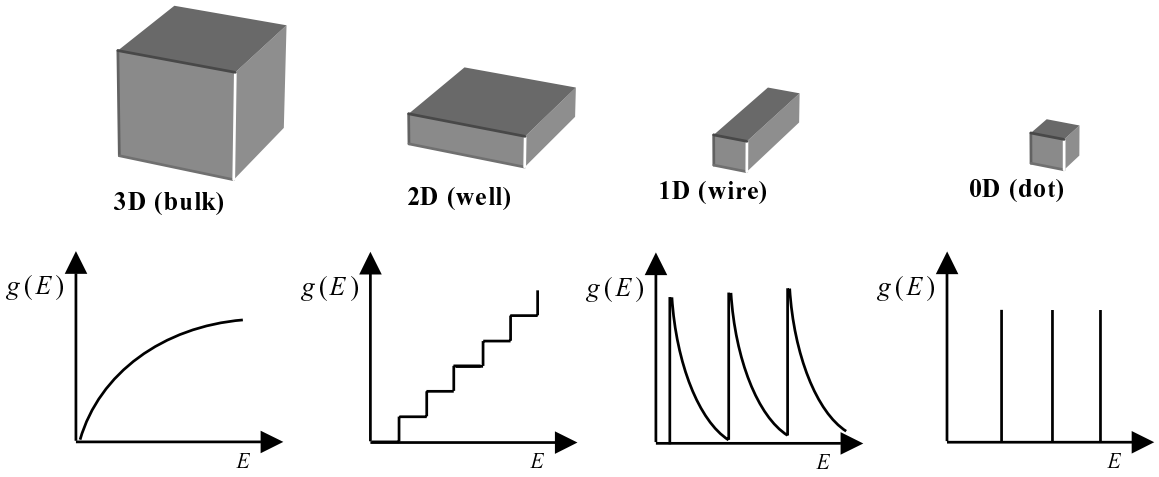

Fig. 1 Densities of states as functions of energies in systems with different numbers of spatial dimensions: 3D, bulk material; 2D, quantum well; 1D, quantum wire; 0D, quantum dot

through the rearrangement of the deposited material when 3D islands are formed. The formation of 3D islands changes completely the strain situation, which will then affect the optoelectronic properties of the quantum dots.

Quantum dots formed in the Stranski-Krastanow mode are called self-assembled dots. The small sizes of the self-assembled quantum dots, the homogeneity of their shapes and sizes in a macroscopic sample, the perfect crystal structure without edge defects, as well as the convenient growth process, without the need for any precise deposition of electrodes or etching, are among their greatest advantages, which stimulate hopes regarding their future application in electronics and optoelectronics, *e.g.*, quantum dot infrared detectors [3,4], quantum dot lasers [5,6] and quantum dot memory devices [7,8].

2. CONTINUUM AND QUANTUM MODELS

In this article, the analysis of the strained semiconductor nanostructures, self-assembled quantum dots (SAQDs), are divided into three parts. First, a linear elastic finite element calculation is performed to determine the strain distribution in and around SAQD nanostructures. Second, the carrier confinement potential in SAQD is modified by the strain distribution. The deformation potential theory is used to estimate the strain-induced potential superimposed to the energy bands of SAQD. Third, a steady-state three-dimensional Schrödinger equation is solved numerically to obtain the energy levels and wave function spectra in the SAQD. Finally, the energy of interband optical transitions is obtained in the numerical experiments.

2.1 Continuum Model

The strain fields inside and in the neighborhood of SAQD strongly affect the electronic properties, and hence the optoelectronic properties, in vicinity of the dots [9,10]. For the optoelectronic properties in III-V semiconductors (such as the materials are InAs and GaAs), there are two predominated strain effects, namely, changes of the conduction band level and the valence band level. The conduction band is only affected by the hydrostatic strain, often referred to as the dilatation or trace of the strain tensor. The valence level can change both with hydrostatic and biaxial strains. In addition, for zinc blende material structures, deviatoric strains give rise to piezoelectrically induced electric fields [11].

To understand the strain effects on optoelectronic properties of QD nanostructures, it is necessary to determine the elastic strain field in the quantum dots and surrounding matrix. There have been various methods in three different main categories: (1) Analytical continuum method [12~14], (2) Continuum finite element method (FEM) [15~18], and (3) Atomistic modeling [19~21]. Analytical continuum method leads to integral expressions for the elastic fields which can be integrated in closed forms for some simplest inclusion shapes, *e.g.*, cylindrical or spherical quantum dots. On the other hand, the interactions between the quantum dot and the surrounding material might have not been fully encountered. FEM is a very versatile and effective numerical method, which have capabilities to easily accommodate various theories and model on QD nanostructures to different levels. Atomistic models might be more reasonable to model systems in nano-scale provided that accurate interatomic potentials are available. Moreover, it requires a huge computing capacity to model quantum dots and the surrounding matrix. In the following sections, we first brief analytical continuum method and continuum finite element method for the QD problems, respectively. Then continuum finite element method will be used to study the SAQD nanostructures for the optoelectronic properties.

2.1.1 Analytical Continuum Method

Analytical continuum methods for calculating the strain and stress distributions attributed to a uniformly strained inclusion were originally developed by Eshelby [22]. From viewpoint of Eshelby's result, a quantum dot can be regarded as an inclusion embedded in an infinite matrix. Due to different lattice constants of the quantum dot and the matrix, the inclusion can be considered as initially strained to accommodate the mismatch in lattice constants. For general cases, having closed forms expression on analytical solutions of stress and strain distributions are not possible, except for some simple geometric shapes such as cubic, cylindrical, spherical, etc. Analytical solutions of the strain field for a buried pyramidal QD structure, including a truncated pyramidal quantum dot and a surrounding matrix, were presented by Pearson [23].

The problem of an initially uniformly strained QD of arbitrary shape embedded in an infinite isotropic medium can be solved analytically by theory of inclusion, under the simplification that both the QD and the matrix have the same elastic moduli. Based on previous works [24,25], a set of vectors has been chosen such that the divergence of each vector gave the Green's function for the stress component σ_{ij}. First, six vectors are defined as follows,

$$\begin{aligned}
\mathbf{A}_{xx}(x,y,z) &= \Lambda x\,\hat{i} \\
\mathbf{A}_{xz}(x,y,z) &= -\Lambda x\,\hat{k} \\
\mathbf{A}_{yy}(x,y,z) &= \Lambda y\,\hat{j} \\
\mathbf{A}_{xy}(x,y,z) &= -\Lambda y\,\hat{i} \\
\mathbf{A}_{zz}(x,y,z) &= \Lambda z\,\hat{k} \\
\mathbf{A}_{yz}(x,y,z) &= -\Lambda z\,\hat{j}
\end{aligned} \tag{1}$$

where

$$\Lambda = \varepsilon_0\, E/[4\pi(1-\nu)(x^2+y^2+z^2)^{3/2}]$$

and ν and E are the Poisson ratio and the Young's modulus, respectively, of the QD and matrix. The misfit strain, ε_0, of the quantum dot is taken with respect to the surrounding matrix; and the quantum dot is assumed to be initially strained by ε_0 in all three directions, namely x-, y-, z-directions. This initial strain is taken as negative for dots, since it is under compression.

The vectors in Eq. (1) are chosen so that $\nabla\cdot\mathbf{A}$ leads to the Green's function stress components σ^{sph} corresponding to a spherical point inclusion. Moreover, the above expressions for $\mathbf{A}$ is not unique because other choices of vectors $\mathbf{A}$ can also yield the Green's function stress components σ^{sph} when taking divergence. For an arbitrary QD shape, the resultant integral to determine the stress σ at the point (x, y, z) is

$$\begin{aligned}
&\sigma_{ij}(x_1, x_2, x_3) \\
&= \int_V \left[\nabla\cdot\mathbf{A}(x_1-x_1^0, x_2-x_2^0, x_3-x_3^0)\right] \mathrm{d}V(x_1^0, x_2^0, x_3^0) \\
&= \int_V \sigma^{sph}(x_1-x_1^0, x_2-x_2^0, x_3-x_3^0)\ \mathrm{d}V(x_1^0, x_2^0, x_3^0) \\
&= \frac{\varepsilon_0 \mathrm{E}}{4\pi(1-\nu)} \int_V \frac{\delta_{ij}r'^2 - 3x_i'x_j'}{r'^5}\ \mathrm{d}V(x_1^0, x_2^0, x_3^0)
\end{aligned} \tag{2}$$

where x_i^0 means points inside V, the volume of the quantum dot, and $x_i' = x_i - x_i^0$, δ_{ij} is the Kronecker delta and $r'^2 = x_i'x_i'$. The summation convention on repeated index has been assumed through this article. Therefore, the solution for a spherical inclusion can be used as a Green's function for the three-dimensional problem. This Green's function was then integrated over the volume of the QD which gives rise to the stress field of the QD.

The analytical stress field of a pyramid QD and a truncated pyramid QD, as illustrated in Fig. 2, can be obtained by evaluating Eq. (2) and expressing in closed form, especially with the aid of any available algebraic software package. The volume of a rectangular-base,

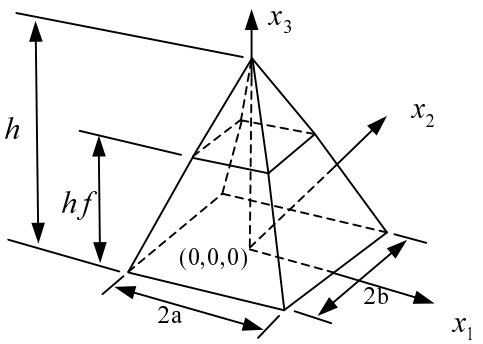

Fig. 2 The geometries of the pyramid and truncated pyramid QD

truncated pyramid QD is defined by,

$$\begin{aligned}
-a\left(1-\frac{x_3^0}{h}\right) &\le x_1^0 \le a\left(1-\frac{x_3^0}{h}\right) \\
-b\left(1-\frac{x_3^0}{h}\right) &\le x_2^0 \le b\left(1-\frac{x_3^0}{h}\right) \\
0 &\le x_3^0 \le hf
\end{aligned} \tag{3}$$

where h means the height of the pyramid QD in the absence of truncation and f represents the degree of truncation, $0 \le f \le 1$. Once each stress component σ_{ij} has been calculated, substituting σ_{ij} into the Hooke's law, of isotropic elastic solids, gives the strain fields:

$$\varepsilon_{ij} = \frac{1}{E}\left[(1+\nu)\sigma_{ij} - \delta_{ij}\nu\sigma_{kk}\right] \tag{4}$$

Equations (2) and (4) enable us to calculate the stress and the strain fields for a single uniformly strained pyramid QD of arbitrary truncation embedded in an infinite medium. For systems containing more than one QD, the principle of superposition of linear problems allows the stresses (strains) at a point to be determined by simply summing the stresses (strain) field of each single QD in the arrays.

Notice that in this analysis, both quantum dots and matrix are assumed as isotropic elastic solids with the same elastic moduli, though it is far away from the reality. Moreover, the QD is assumed to be deformed initially only without any further elastic deformation. The full interaction between QD and the matrix may have not been taken into account properly. Besides, the matrix is assumed to be of unbounded extent; hence effects of free surfaces have not yet been included in this formulation.

2.1.2 Continuum Finite Element Method

Another important category of methods on

computing the stress and strain fields induced by QD is the continuum finite element method (FEM). FEM gives only the numerical results for quantum dots. On the other hand, it works even for rather complex geometries, and provides a complete picture of the strain distribution of a three-dimensional model. In addition, assumptions of isotropic as well as same elastic moduli as in previous methods are not needed here. Furthermore, with the improvement of computer technology, it becomes much easier even to handle heavy tasks, especially 3D (three dimension) problems with FEM. Benabbas [26] and Muralidharan [16] gave a 2D (two dimension) axisymmetric model to analyze the strain distribution inside and in the neighborhood of QD. A 3D model for strain field was presented in [27].

Notice that the mismatch of lattice constants will induce further elastic deformation in the whole nanostructure system, namely, in both the substrate and the quantum dot island. In other words, the lattice mismatch will not be the only strain in the quantum dot island. In these works, the lattice mismatch between dot and substrate is simulated under the framework of the theory of thermo-elasticity. For these calculations, both QD and substrate are assigned to have corresponding hypothetical coefficients of thermal expansion, in order to produce a desired misfit across the interface matching the initial strain from lattice-mismatched. For example, growing InAs on (001) GaAs substrate by molecular beam epitaxy (MBE) results in pyramid-like islands (dots) [28~30]. The lattice mismatch between InAs and GaAs is about 6.7%. The initial strain field induced by lattice mismatch can then be simulated by setting the hypothetical coefficient of thermal expansion of the DQ and the substrate to be as $0.067°K^{-1}$and 0, respectively, with a raised temperature by 1°K.

In the numerical experiments of this article, a buried pyramidal InAs/GaAs SAQD nanostructure, as depicted schematically in Fig. 3, is considered. The InAs dot is self-assembled under certain conditions during heteroepitaxy on (001) GaAs substrates on which a thin wetting layer is grown first, followed by coherent island formation. The dot is subsequently covered by additional substrate materials. Epitaxially grown semiconductor heterostructures, such as SAQDs, often consist of several materials with different lattice constants. The mismatch of lattice constants gives rise to the strain field in a QD nanostructure, which will then affect the optoelectronic properties of the quantum dots. The model based on the linear elasticity theory will be developed to evaluate the strain distribution in and around the InAs/GaAs SAQD nanostructure.

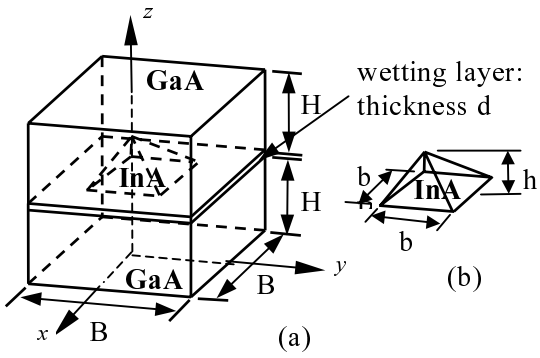

Fig. 3 Schematics of (a) the buried InAs/GaAs QD nanostructure : B = 30nm, H = 30nm, d = 0.5nm, and (b) the island (InAs dot) b = pyramid width, h = pyramid height

In-plane (the base plane of QD) lattice mismatch parameter is usually defined as

$$(\varepsilon_0)_{xx} = (\varepsilon_0)_{yy} = \frac{a_s - a_d}{a_d} \tag{5}$$

where a_s and a_d are the lattice constants of the substrate material and the QD, respectively. Notice that the mismatch of lattice constants will induce further elastic deformation in the whole nanostructure system, namely, in both the substrate and the QD island. In other words, the lattice mismatch parameter defined in Eq. (5) will not be the only strain in the quantum dot island, it will instead be treated as in-plane initial strain in the latter finite element analysis. On the other hand, the out-of-plane initial strain has never yet been as conclusive as its in-plane counterparts. In this article, the out-of-plane initial strain is set to zero such that the initial strain tensor is given as

$$\boldsymbol{\varepsilon}_0 = \begin{bmatrix} (\varepsilon_0)_{xx} & 0 & 0 \\ 0 & (\varepsilon_0)_{yy} & 0 \\ 0 & 0 & 0 \end{bmatrix} \tag{6}$$

Based on the theory of linear elasticity, the stress-strain relation of anisotropic solids with initial strains can be written as:

$$\boldsymbol{\tau}_{ij} = C_{ijkl}[\boldsymbol{\varepsilon}_{kl} - (\boldsymbol{\varepsilon}_0)_{kl}] \qquad i, j, k, l = x, y, z \tag{7}$$

where τ_{ij} and ε_{kl} are the stress and total strain tensors, respectively. C_{ijkl} is the elastic moduli tensor, and $(\varepsilon_0)_{kl}$ is the initial strain tensor defined in Eq. (6). Here both GaAs and InAs are treated as cubic materials with 3 independent elastic moduli each. A list of material properties used, including lattice constants and elastic moduli, is summarized in Table 1.

Table 1 Material properties

Mechanical property	a_0 (nm)	C_{11} (GPa)	C_{12} (GPa)	C_{44} (GPa)
GaAs	0.565	118.79	53.76	59.4
InAs	0.605	83.29	45.26	39.6

Deformation potential	a_c (eV)	a_v (eV)	b (eV)
GaAs	−7.17	1.16	−1.7
InAs	−5.08	1	−1.8

Effective mass[a]	$m_e(m_0)$	$M_{hh,xy}(m_0)$	$M_{hh,z}(m_0)$
GaAs	0.067	0.115	0.333
InAs	0.023	0.035	0.263

[a]From Luttinger-Kohn parameters $\gamma_1, \gamma_2, \gamma_3$

The linear elasticity boundary value problem, arising from the mismatch in lattice constants between the wetting layer, QD island and substrate materials, is analyzed, here, using a commercial finite element package FEMLAB. Appropriate boundary conditions are needed in the analysis: all the nodes of the outer surfaces parallel to the x- and y-outer surfaces are fixed in the normal displacement due to periodic symmetric argument. The bottom outer surface is fixed against displacement in z-direction to avoid rigid body shift; whiles the upper surface is kept traction free. The displacement compatibility across the interface of island/ substrate is satisfied automatically in the finite element formulation with displacement field as unknowns.

It is worthwhile to point out that the wetting layer and QD island grew on the substrate and embedded within the capping layer, as depicted in Fig. 3. In the conventional analysis, the capping layer is assumed to be deformed together with QD and substrate. On the other hand, in fact, in the fabrication process, the capping layer is deposited after the QD has been deformed to compensate the mismatch of lattice constants. Hence the capping layer should have never been experienced the deformation of QD at all, in fabrication process. To take this sequence of fabrication process into account, in this article, the capping layer is added into the nanostructure system only after the strain analysis of quantum dot and substrate has been completed, and is assumed to be unstrained thereafter. After the strain field has been calculated, the capping layer is added when solving the Schrödinger equation. This is equivalent to assume that the strain distribution in the QD does not to affect the capping layer.

It is also of interest to point out that QDs are grown in a large array instead of a single dot actually. In a finite element model, it is easy to consider a single dot or a regular array of dots. However, the strain distribution within a disordered array of dots will still be impractical, if not impossible, to be obtained by using finite element methods. FEM is rather computationally intense compared to analytic solutions. To obtain results to certain accuracy, the grid size must be kept small enough; however, as the grid size is reduced, the demand on computational memory and time increases rapidly. The choice of the grid size depends on the accuracy required and computer capacity and time available.

2.2 Quantum Model

The band structure is determined by considering the difference in band gap energies of the heterostructure constituent materials. A part of band gap difference is taken up by a conduction band offset, and a portion results in a valence band offset, as shown in Fig. 4, for the cases that QD and substrate are taken as InAs and GaAs, respectively.

The strain effects will induce an extra potential field, V_{strain}. For the strained QD nanostructure, the confinement potential can be written as a sum of energy offsets of the conduction band (or valence band), V_{band}, and the strain-induced potential, V_{strain}, as

$$V(\vec{r}) = V_{\text{band}}(\vec{r}) + V_{\text{strain}}(\vec{r}) \tag{8}$$

The strain contribution to the potential is determined via deformation potential theory, modified by the strain tensor ε_{ij}. It may then affect the energy band structure for the QD, altering further optoelectronic properties in the devices.

Here, Pikus-Bir Hamiltonian [9,10] together with the computed strain field from above-mentioned strain field calculations (section 2.1.2) are used to determine strain-induced potentials in QD. It is known that the conduction band level will be only affected by the hydrostatic strain [11], and the strain-induced potential for the conduction band can be expressed as [9]

$$V^c_{\text{strain}} = a_c\,(\varepsilon_{xx} + \varepsilon_{yy} + \varepsilon_{zz}) \tag{9}$$

On the other hand, the valence level can be changed with not only hydrostatic strain but also biaxial strain. The strain-induced potential for the valence band can then be written as [10]

$$V_{\text{strain}}^{v} = a_v(\varepsilon_{xx}+\varepsilon_{yy}+\varepsilon_{zz}) - \frac{b}{2}(\varepsilon_{xx}+\varepsilon_{yy}-2\varepsilon_{zz}) \quad (10)$$

where a_c is the deformation potential constant of conduction band; while a_v and b denote the deformation potential constants of valence band. The data of these three constants for InAs and GaAs are summarized in Table 1. The strain-induced potentials are computed according to Eqs. (9) and (10) and are superimposed to energy band. In our cases, all other potential energy contributions, such as piezoelectric potential energy, are expected to be small and are neglected in the calculations.

The behavior of individual carrier in QD nanostructures is governed by the three-dimensional steady state Schrödinger equation as:

$$\left[-\frac{\hbar^2}{2}\nabla_{\vec{r}}\left(\frac{1}{m^*}\right)\nabla_{\vec{r}} + V(\vec{r})\right]\psi_n(\vec{r}) = E_n\,\psi_n(\vec{r}) \quad (11)$$

Equation (11) is solved numerically again, in this article, by means of a commercial finite element method package, FEMLAB, to obtain energy levels and the wave functions in a QD nanostructure. The boundary conditions on the quantum dot/substrate interfaces are

$$\begin{cases} \psi_d = \psi_s \\ \dfrac{1}{m^*_{d_{n_i}}}\dfrac{d\psi_d}{dn} = \dfrac{1}{m^*_{s_{n_i}}}\dfrac{d\psi_s}{dn} \end{cases} \quad (12)$$

where subscripts d and s denote the QD and substrate regions, respectively, n denotes the normal directions of interfaces, and a carrier effective mass is taken along the normal directions of interfaces. In addition, at the top of the capping layer, bottom of the substrate, and their outer surfaces, the wave function is set to zero.

Based on the computed energy and wave function distributions, the energy of interband optical transitions can readily be obtained. The optical conductivity features peaks at particular wavelengths of light that are more strongly absorbed; these wavelengths in turn can be expected to be the strongest emission wavelengths.

2.3 Numerical Results

The geometry of an embedded InAs/GaAs QD nanostructure considered here is depicted in Fig. 4; the

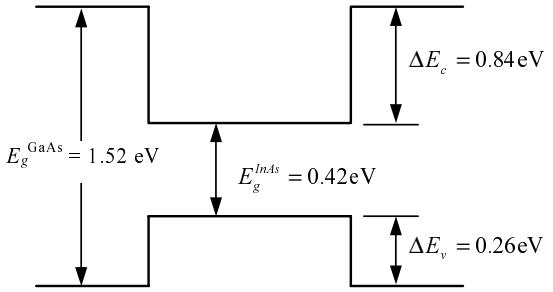

Fig. 4 Initial energy band of the unstrained InAs/GaAs heterostructure used for quantum dot calculations

Table 2 Dimensions of the QD nanostructures

Structure	I	II	III	IV	V
width b (nm)	12	12	12	16	20
height h (nm)	3	4	6	6	6

InAs QD is assumed to be as pyramidal shape with square-based of width b. Sizes of QD used in the numerical experiments of the article are listed in Table 2. The semiconductor materials are treated as anisotropy during the strain analysis. As mentioned in section 2.1.2, since the capping layer does not experience the deformation of QD in the self-assembled process; in the stage of strain analysis, the QD heterostructure system is considered to consist of only quantum dot, wetting layer and substrate but not capping material. Once the strain analyses have been completed, the capping layer is then added into the system. The adding of capping material is only for the purpose of solving the Schrödinger equation to obtain the electronic structure of the nanostructure system.

In this model, the capping layer is consequently assumed to be unstrained. The model takes the sequence of fabrication process into account. It is equivalently to neglect the re-distribution of strain in

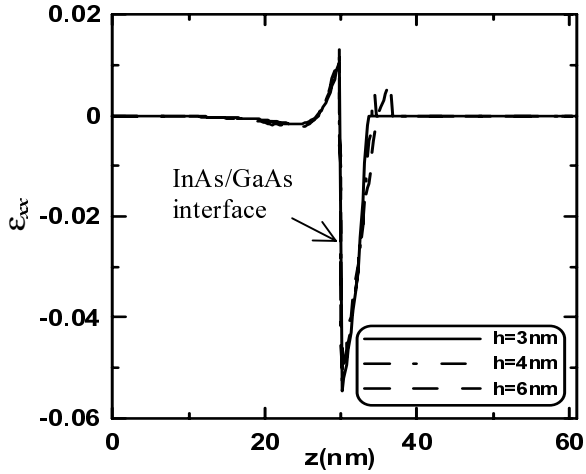

Fig. 5 Strain components ε_{xx} plotted along the z-axis for structure I, II, and III

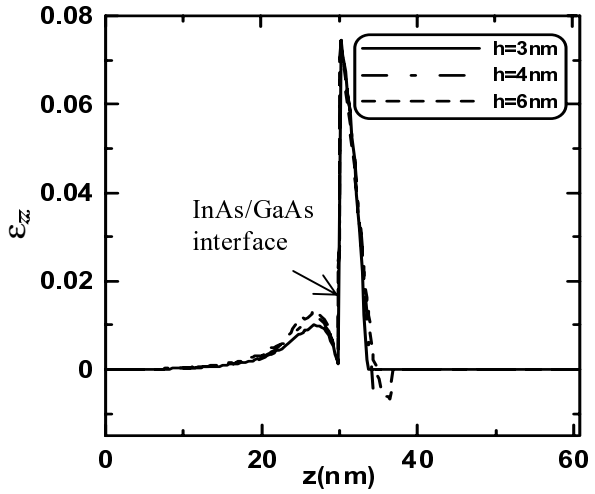

Fig. 6 Strain components ε_{zz} plotted along the z-axis for structure I, II, and III

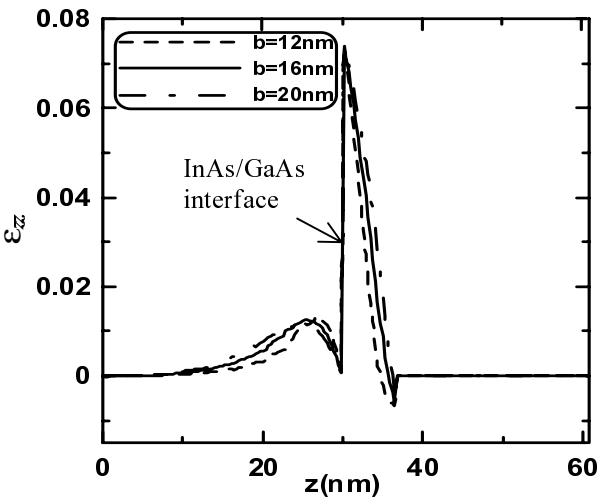

Fig. 8 Strain components ε_{zz} plotted along the z-axis for structure III, IV, and V

the QD system during the depositing process of the capping layer, which is expected to be much small compared to the strain distribution in the QD and in the substrate material.

Strain components ε_{xx} and ε_{zz}, are shown in Figs. 5 and 6, respectively, along z-axis in QD structures for the cases of width b = 12nm with various heights (h = 3, 4, and 6nm). These strain components show ample discontinuities across the interface of InAs wetting layer and the GaAs substrate (*i.e.* InAs/GaAs interface), as one would expect. Moreover, the strain field ε_{xx} inside the QD is compressive while ε_{zz} is tensile. These reflect the fact that the lattice constant of InAs is larger than that of GaAs. Similarly, strain components ε_{xx} and ε_{zz}, are shown in Figs. 7 and 8, respectively, along z-axis in QD structures for the cases of height h = 6nm with various widths (b = 12, 16, and 20nm).

From Figs. 5 ~ 8, it is easily to conclude that strain

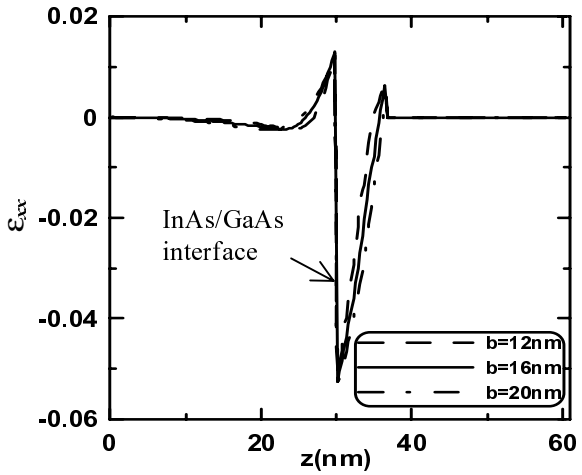

Fig. 7 Strain components ε_{xx} plotted along the z-axis for structure III, IV, and V

fields are larger for larger QD size, as one would expect, since a larger QD can be viewed as a larger source of initial-strain field.

The calculated ground state energy level and corresponding transition energy in the QD nanostructure are summarized in Table 3. The transition energy is defined as the energy difference between the electron and the hole. The peak of experimental photoluminescence (PL) spectra is related to the transition energy. From the numerical results in Table 3, it is seen that the energy of interband optical transition becomes smaller as the island size increasing. This phenomenon agrees well with the previous experimental photoluminescence data [31].

Probability density function profiles, given by square of wave functions, namely $|\psi|^2$, for the ground state energy levels in the QD nanostructures, are shown in Fig. 9. Subfigures 9(a) and 9(b) are the probability density function profiles corresponding to electron and hole, respectively, energy levels for the structure I (h = 3nm). Similarly, subfigures 9(c) and 9(d) are for the case of the structure III, namely h = 6nm. It is easily to see that, from Fig. 9, the probability density function distributions are confined almost entirely to the island region. Moreover, the probability density function distributions of electrons appear to be spherical symmetry within the whole island, subfigures 9(a) and 9(c). On the other hand, the probability density function distributions of hole are likely to be more confined in the bottom of the island, subfigures 9(b) and 9(d).

Similarly, Fig. 10 shows the probability density function profiles of the first excited energy levels of the electron and the hole. Again, subfigures 10(a) and 10(b) correspond to the electron and to the hole, respectively, for the case of h = 3nm; while subfigures

Table 3 Ground state energy level and the transition energy (eV)

	Electron energy	Hole energy	Transition energy
Structure I	1.302	0.203	1.099
Structure II	1.239	0.216	1.023
Structure III	1.150	0.229	0.921
Structure IV	1.113	0.268	0.845
Structure V	1.095	0.295	0.800

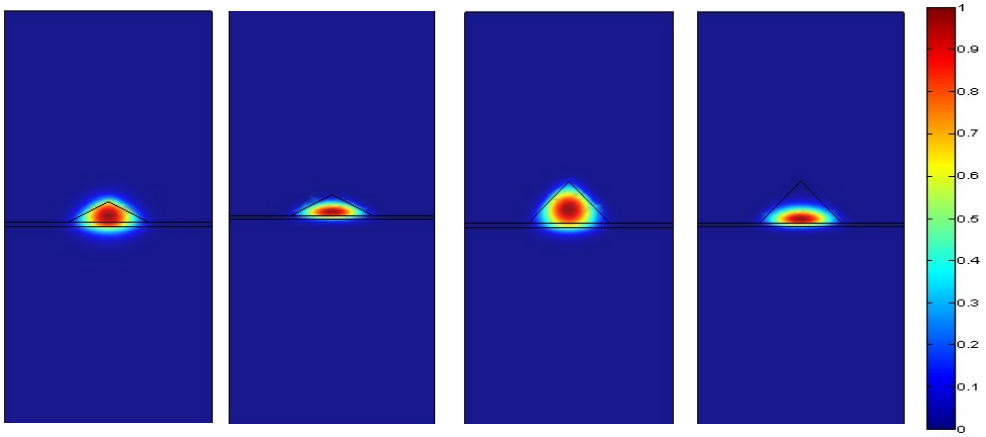

Fig. 9 Probability density function profiles for energy levels of the ground state in the *yz*-plane through the dot center. For QD structure I: (a) electron energy; (b) hole energy. For QD structure III: (c) electron energy; (d) hole energy

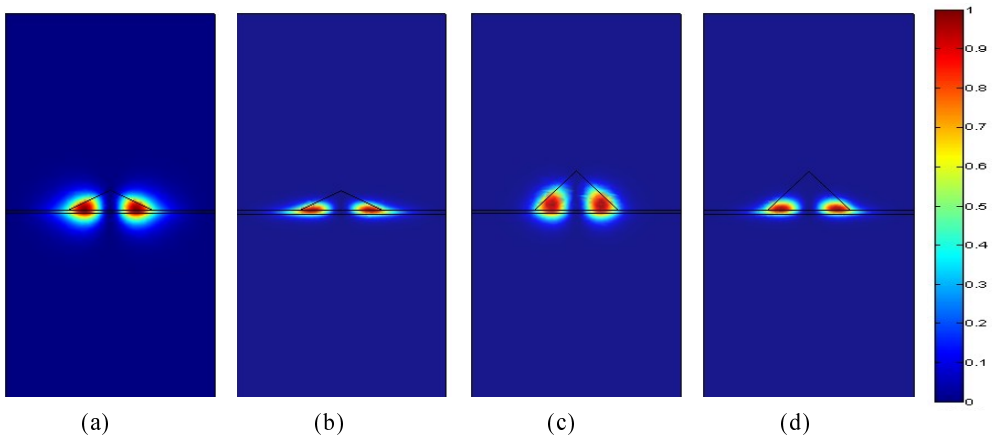

Fig. 10 Probability density function profiles for energy levels of the first excited in the *yz*-plane through the dot center. For QD structure I: (a) electron energy; (b) hole energy. For QD structure III: (c) electron energy; (d) hole energy

10(c) and 10(d) are for the case of h = 6nm. Compared to probability density function distributions of the ground state, namely to the Fig. 9, the ones of first excited state are confined more at the corner of quantum dot.

The calculated transition energies range from 1.1 eV to 0.8 eV which correspond to 1128nm and 1550nm in the optical wavelength spectrum. This wavelength spectra spread in the infrared radiation.

3. CONCLUSIONS

In this article, a model has been presented for analyzing mechanical and optoelectronic coupling in the pyramidal InAs/GaAs SAQD nanostructure. The model is based on theory of linear elasticity and has taken the sequence of the fabrication process into account to analyze three-dimensional induced strain field by mismatch of lattice constants in quantum dots.

Further, the energy levels and wave function distributions in SAQD nanostructures have also been studied by solving the steady state three-dimensional effective mass Schrödinger equation. The effects of the strain-induced potential have been considered through Pikus-Bir Hamiltonian. Finally energies of interband optical transitions are obtained in numerical experiments.

In the article, the fact that transition energy decreases with increasing the quantum dot size has been revealed through numerical computation. This phenomenon agrees well with the previous results reported by others. The wavelengths of the optical transition energies in pyramidal InAs/GaAs SAQD nanostructures considered in the article range from 1128 nm to 1550 nm in the optical wavelength spectrum. The wavelength spectra will be mostly attractive in the applications of optical fiber communications. The InAs/GaAs SAQD nanostructures would have great potential in future optical applications.

ACKNOWLEDGMENTS

This work is carried out in the course of research sponsored by the National Science Council of Taiwan under Grant No. NSC92-2212-E-002-072.

REFERENCES

[1] S. S. Iyer, G. L. Patton, J. M. C. Strok, B. S. Meyerson and D. L. Harame, "Heterojunction bipolar transistors using Si-Ge Alloys," *IEEE Trans. Electron Devices*, 1989, p. 2043.

[2] E. Bauer and J. H. van der Merwe, "Structure and growth of crystalline superlattices: From monolayer to superlattice," *Phys. Rev. B*, Vol. 33, 1986, p. 3657.

[3] S. Maimon, E. Finkman, G. Bahir, S. E. Schacham, J. M. Garcia and P. M. Petroff, "Intersublevel transitions in inAs/GaAs quantum dots infrared photodetectors," *Appl. Phys. Lett.*, Vol. 73, 1998, p. 2003.

[4] J. L. Jiminez, L. R. C. Finseca, D. J. Brady, J. P. Leburton, D. E. Wohlert and K. Y. Cheng, "The quantum dot spectrometer," *Appl. Phys. Lett.*, Vol. 71, 1997, p. 3558.

[5] L. Harris, D. J. Mawbray, M. S. Skolnick, M. Hopkinson and G. Hill, "Emission spectra and mode structure of InAs/GaAs self-organized quantum dot lasers," *Appl. Phys. Lett.*, Vol. 73, 1998, p. 969.

[6] D. L. Huffaker, G. Park, Z. Zou, O. B. Shchekin and D. G. Deppe, "Discrete energy level separation and the threshold temperature dependence of quantum dot Lasers," *Appl. Phys. Lett.*, Vol. 73, 1998, p. 2564.

[7] J. J. Finley, M. Skalitz, M. Arzberger, A. Zrenner, G. Bohm and G. Abstreiter, "Electrical detection of qptically induced charge storage in Self-Assembled InAs quantum dots," *Appl. Phys. Lett.*, Vol. 73, 1998, p. 2618.

[8] Amlani, A. O. Orlov, G. L. Snider, C. S. Lent and G. Bernstein, "Demonstration of a Six-Dot quantum cellular automata system," *Appl. Phys. Lett.*, Vol. 72, 1998, p. 2179.

[9] G. E. Pikus and G. L. Bir, "Effects of deformation on the hole energy spectrum of gernasium and silicon," *Sov. Phys. Solid State*, Vol. 1, 1960, pp. 1502–1517.

[10] G. E. Pikus and G. L. Bir, *Symmetry and Strain-Induced Effects in Semiconductors*, Wiley New York, 1974.

[11] S. L. Chuang, *Physics of optoelectronic devices*, John Wiley & Sons, New York, 1995.

[12] V. A. Shchukin, D. Bimberg, V. G. Malyshkin and N. N. Ledentsov, "Vertical correlations and anticorrelations in multisheet arrays of two dimensional islands," *Phys. Rev., B*, Vol. 57, 1998, p. 12262.

[13] D. Andreev, J. R. Downes, D. A. Faux and E. P. O'Reilly, "Strain distributions in quantum dots of arbitrary shape," *J. Appl. Phys.*, Vol. 86, 1999, p. 297.

[14] G. S. Pearson and D. A. Faux, "Analytical solutions for strain in pyramidal quantum dots," *J. Appl. Phys.*, Vol. 88, 2000, p. 730.

[15] T. Benabbas, Y. Androussi and A. Lefebvre, "A finite element study of strain fields in vertically aligned inas islands in gaAs," *J. Appl. Phys.*, Vol. 86, 1999, p. 1945.

[16] G. Muralidharan, "Strains in InAs quantum dots embedded in GaAs: A finite element study," *Jpn. J. Appl. Phys.*, Vol. 39, 2000, L 658.

[17] H. T. Johnson, L. B. Freund, C. D. Akyüz and A. Zaslavsky, "Finite element analysis of strain effects on electronic and transport properties in quantum dots and wires," *J. Appl. Phys.*, Vol. 84, 1998, p. 3714.

[18] L.B. Freund and H.T. Johnson, "The influence of strain on confined electronic states in semi-conductor quantum structures," *J. Mech. Phys. Solids*, Vol. 38, 2001, p. 1045.

[19] M. Tadic, F. M. Peeters, K. L. Janssens, M. Korkusinski and P. Hawrylak, "Strain and band edges in single and coupled cylindrical inas/ gaas and inp/ingap self-assembled quantum dots," *J.*

Appl. Phys., Vol. 92, 2002, p. 5819.

[20] C. Pryor, J. Kim, L. W. Wang, A. J. Williamson and A. Zunger, "Comparison of two methods for describing the strain profiles in quantum dots," *J. Appl. Phys.*, Vol. 83, 1998, p. 2548.

[21] M. E. Bachlechner, A. Omeltchenko, A. Nakano, R. K. Kalia, P. Vashishta, I. Ebbsjö, A. Madhukar and P. Messina, "Multimillion-Atom molecular dynamics simulation of atomic level stresses in Si(111)/Si3N4(0001) nanopixels," *Appl. Phys. Lett.*, Vol. 72, 1998, p. 1969.

[22] J. D. Eshelby, "The Determination of the Elastic Field of an Ellipsoidal Inclusion and Related Problems," *Proc. R. Soc. London*, Ser. A 241, 1957, pp. 376.

[23] G. S. Pearson and D. A. Faux, "Analytical solutions for strain in pyramidal quantum dots," *J. Appl. Phys.*Vol. 88, 2000, P. 730.

[24] D. A. Faux, J. R. Downes and E. P. O'Reilly, "A simple method for calculating strain distributions in quantum wire structures," *J. Appl. Phys.*, Vol. 80, 1996, p. 251.

[25] J. R. Downes, D. A. Faux and E. P. O'Reilly, "A simple method for calculating strain distributions in quantum dot structures," *J. Appl. Phys.*, Vol. 81, 1997, p. 6700.

[26] T. Benabbas, P. Francois, Y. Androussi and A. Lefebvre, "Stress relaxation in highly strained inas/gaas structures as studied by finite element analysis and transmission electron microscopy," *J. Appl. Phys.*, Vol. 80, 1996, p. 2763.

[27] G. R. Liu and S. S. Quek Jerry, "A finite element study of the stress and strain fields of inas quantum dots embedded in GaAs," *Semicond. Sci. Technol.*, Vol. 17, 2002, p. 630.

[28] M. Geiger, A. Bauknecht, F. Adler, H. Schweizer and F. Scholz, "Observation of the 2D-3D growth mode transition in the InAs/GaAs system," *J. Grys. Growth*, Vol. 170, 1997, p. 558.

[29] S. Ruvimov, P. Werner, K. Scheerschmidt, U. Gosele, J. Heydenrenich, U. Richter, N. N. Ledentsov, M. Grundmann, D. Bimberg, V. M. Ustinov, A. Y. Egorov, P. S. Kop'ev and Z. I. Alferov, "Structural characterization of (In,Ga) as quantum dots in a GaAs matrix," *Phys. Rev. B*, Vol. 51, 1995, p. 14766.

[30] D. Bimberg, M. Grundmann, N. N. Ledentsov, S. Ruvimov, P. Werner, U. Richter, J. Heydenrenich, V. M. Ustinov, P. S. Kop'ev and Z. I. Alferov, "Self-Organization processes in MBE-Grown quantum dot structures," *Thin Solid Films*, Vol. 267, 1995, p. 32.

[31] F. Heinrichsdorff, A. Krost, M. Grundmann, D. Bimberg, F. Bertram, J. Christen, A. Kosogov and P. Werner, "Self organization phenomena of InGaAs/GaAs quantum dots grown by metalorganic chemical vapour deposition," *J. Crys. Growth*, Vol. 170, 1997, p. 568.

Tzy-Rong Lin (林 資 榕) is currently a Ph.D. candidate of Applied Mechanics at the National Taiwan University, Taipei, Taiwan. His research is mainly in the area of mechanical and optoelectronic coupling in semiconductor nanostructures.

Mao-Kuen Kuo (郭 茂 坤) received his B.S. and M.S. degrees in civil engineering from National Taiwan University, Republic of China, in 1977 and 1979, respectively, and Ph.D. degree in civil engineering from Northwestern University, United States of America, in 1984.
Presently, he is a Professor in the Institute of Applied Mechanics, National Taiwan University. He joined the faculty of National Taiwan University in 1984. His research work is mainly on Elastodynamic Fracture Mechanics and Nondestructive Evaluation. He was a recipient of the 1987 Teaching Award sponsored by the Ministry of Education, Republic of China. He was also recipients of the 1987, 1988, 1989 and 2002 Teaching Award sponsored by the College of Engineering, National Taiwan University.

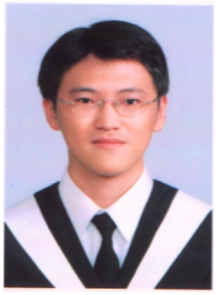

Bo-Ting Liao (廖 柏 亭) received the B.S. degree in mechanical engineering from the National Cheng Kung University, Tainan, in 2002. He now studies the M.S. degree in Institute of Applied Mechanics, National Taiwan University, Taipei, Taiwan. His research focuses on the mechanical and optoelectronic properties of nanostructures.

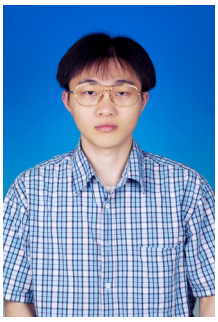

Kuo-Pin Hung (洪 國 彬) received the M.S. degree in Institute of Applied Mechanics at the National Taiwan University, Taipei, Taiwan in 2003. He is now a Ph.D. student in Institute of Applied Mechanics, National Taiwan University. His research is mainly on the piezoelectric mechanics and electronic properties of semiconductor.

收稿日期 93 年 5 月 10 日、修訂日期 93 年 5 月 23 日、接受日期 93 年 5 月 27 日
Manuscript received May 10, 2004, revised May 23, 2004, accepted May 27, 2004